Beampattern Design

J. Benesty, I. Cohen, and J. Chen,
Fundamentals of Signal Enhancement and Array Signal Processing,
Wiley-IEEE Press, 2017.

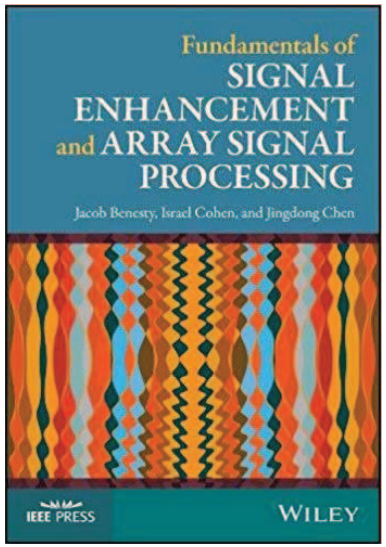

Outline

Introduction

For simplicity, we assume that we have a uniform linear array (ULA).

Because of the symmetry of the steering vector associated with a ULA, the only directions where we can design any symmetric beampattern are at the endfires (i.e., 0 and π).

Since we are interested in frequency-invariant beampatterns, the distance between two successive sensors must be small.

The beampatterns that we propose to design in this talk are similar to the ones obtained with differential sensor arrays (DSAs).

After revisiting the definitions of the beampatterns and showing some relationships, we explain different techniques for beampattern design.

Beampatterns Revisited

Theoretical DSA Beampattern

The beampattern corresponding to the filter $\mathbf{h}(f)$, of length M, applied to a ULA is

$$\begin{aligned}\mathcal{B}\left[\mathbf{h}(f), \cos\theta\right] &= \mathbf{d}^H\left(f, \cos\theta\right)\mathbf{h}(f) \\ &= \sum_{m=1}^{M} H_m(f) e^{\jmath \overline{f}_m \cos\theta},\end{aligned} \tag{1}$$

where we define

$$\overline{f}_m = \frac{2\pi\delta}{c}(m-1)f = 2\pi\tau_0(m-1)f \tag{2}$$

to simplify the notation.

We recall that $\mathbf{h}(f)$ is designed so that the array looks in the direction $\theta = 0$ (or $\theta = \pi$).

For a fixed $\mathbf{h}(f)$, it is obvious that $\mathcal{B}\left[\mathbf{h}(f), \cos\theta\right]$ is even and periodic with respect to the variable θ, i.e.,

$$\mathcal{B}\left[\mathbf{h}(f), \cos\left(-\theta\right)\right] = \mathcal{B}\left[\mathbf{h}(f), \cos\theta\right] \tag{3}$$

and

$$\mathcal{B}\left[\mathbf{h}(f), \cos\left(\theta + 2\pi\right)\right] = \mathcal{B}\left[\mathbf{h}(f), \cos\theta\right]. \tag{4}$$

As a result, the study and design of a desired beampattern is limited to $\theta \in [0, \pi]$.

Let $\mathcal{B}\left(\theta\right)$ be a real even periodic function with period 2π and such that $\int_0^\pi \left|\mathcal{B}\left(\theta\right)\right| d\theta$ exists, then it is well known that $\mathcal{B}\left(\theta\right)$ can be written in terms of its Fourier cosine series [1]:

$$\mathcal{B}\left(\theta\right) = \sum_{n=0}^{\infty} b_n \cos\left(n\theta\right), \tag{5}$$

where

$$\begin{cases} b_0 = \dfrac{1}{\pi}\displaystyle\int_0^{\pi} \mathcal{B}(\theta)\, d\theta \\ \\ b_i = \dfrac{2}{\pi}\displaystyle\int_0^{\pi} \mathcal{B}(\theta)\cos(i\theta)\, d\theta, \quad i \geq 1 \end{cases}.$$

Now, if we limit this series to the order N, $\mathcal{B}(\theta)$ can be approximated by [2], [3]

$$\begin{aligned} \mathcal{B}(\mathbf{b}_N, \cos\theta) &= \sum_{n=0}^{N} b_{N,n}\cos(n\theta) \\ &= \mathbf{b}_N^T \mathbf{p}_{\mathrm{C}}(\cos\theta), \end{aligned} \tag{6}$$

where $b_{N,n},\ n = 0, 1, \ldots, N$ are real coefficients and

$$\mathbf{b}_N = \begin{bmatrix} b_{N,0} & b_{N,1} & \cdots & b_{N,N} \end{bmatrix}^T,$$
$$\mathbf{p}_{\mathrm{C}}(\cos\theta) = \begin{bmatrix} 1 & \cos\theta & \cdots & \cos(N\theta) \end{bmatrix}^T,$$

are vectors of length $N + 1$.

The function $\mathcal{B}(\mathbf{b}_N, \cos\theta)$ is, in fact, a very general definition of a frequency-independent directivity pattern of order N.

It is very much related to the directivity pattern of the Nth-order DSA:

$$\mathcal{B}(\mathbf{a}_N, \cos\theta) = \sum_{n=0}^{N} a_{N,n} \cos^n\theta = \mathbf{a}_N^T \mathbf{p}(\cos\theta), \tag{7}$$

and any DSA beampattern can be designed with $\mathcal{B}(\mathbf{b}_N, \cos\theta)$.

Indeed, we know from the usual trigonometric identities that

$$\cos^n \theta = \sum_i b(n,i) \cos\left[(n-2i)\,\theta\right], \tag{8}$$

where $b(n,i)$ are some binomial coefficients.

Substituting (8) into (7), we deduce that any DSA beampattern can be written as a general beampattern, $\mathcal{B}\left(\mathbf{b}_N, \cos\theta\right)$.

It is well known that

$$\cos\left(n\theta\right) = T_n\left(\cos\theta\right), \tag{9}$$

where $T_n\left(\cdot\right)$ is the nth Chebyshev polynomial of the first kind [4], which have the recurrence relation:

$$T_{n+1}\left(\cos\theta\right) = 2\cos\theta \times T_n\left(\cos\theta\right) - T_{n-1}\left(\cos\theta\right), \tag{10}$$

with

$$\begin{cases} T_0(\cos\theta) = 1 \\ T_1(\cos\theta) = \cos\theta \end{cases}.$$

Thus, $\cos(n\theta)$ can be expressed as a sum of powers of $\cos\theta$.

Consequently, any general beampattern can be written as a DSA beampattern.

We can then conclude that $\mathcal{B}(\mathbf{b}_N, \cos\theta)$ and $\mathcal{B}(\mathbf{a}_N, \cos\theta)$ are strictly equivalent.

An even more general definition of a frequency-independent beampattern with orthogonal polynomials can be found in [5].

Basically, this shows that any even periodic function (here a desired beampattern) can be designed or approximated with its Fourier

cosine series, which also corresponds to the theoretical Nth-order DSA beampattern.

For convenience, we give the relations between the coefficients $b_{N,n},\ n = 0, 1, \ldots, N$ of $\mathcal{B}(\mathbf{b}_N, \cos\theta)$ and the coefficients $a_{N,n},\ n = 0, 1, \ldots, N$ of $\mathcal{B}(\mathbf{a}_N, \cos\theta)$ for the first three orders:

- $N = 1$: $b_{1,0} = a_{1,0}$, $b_{1,1} = a_{1,1}$;
- $N = 2$: $b_{2,0} = a_{2,0} + \frac{a_{2,2}}{2}$, $b_{2,1} = a_{2,1}$, $b_{2,2} = \frac{a_{2,2}}{2}$; and
- $N = 3$: $b_{3,0} = a_{3,0} + \frac{a_{3,2}}{2}$, $b_{3,1} = a_{3,1} + \frac{3a_{3,3}}{4}$, $b_{3,2} = \frac{a_{3,2}}{2}$, $b_{3,3} = \frac{a_{3,3}}{4}$.

Beampattern Design

Now, in order to be able to design any desired beampattern, $\mathcal{B}\left(\mathbf{b}_N, \cos\theta\right)$, with $\mathcal{B}\left[\mathbf{h}(f), \cos\theta\right]$, where $\mathbf{h}(f)$ needs to be found accordingly, we have to approximate the exponential function that appears in (1) in terms of Chebyshev polynomials as it will become clearer soon.

Since the complex-valued exponential function is infinitely differentiable and even with respect to the variable θ, we can find the complex-valued coefficients $c_n,\ n = 0, 1, 2, \ldots$ such that

$$e^{\jmath \overline{f}_m \cos\theta} = \lim_{N\to\infty} \sum_{n=0}^{N} c_n \cos\left(n\theta\right). \tag{11}$$

By limiting the above series to a fixed N, we propose to find the coefficients $c_n,\ n = 0, 1, \ldots, N$ in the best possible way in a least-squares error (LSE) sense, i.e., by minimizing the criterion:

$$\begin{aligned}
\mathrm{LSE}\left(\mathbf{c}_N\right) &= \frac{1}{\pi}\int_0^\pi \left| e^{-\jmath \overline{f}_m \cos\theta} - \sum_{n=0}^{N} c_n^* \cos\left(n\theta\right)\right|^2 d\theta \qquad (12)\\
&= \frac{1}{\pi}\int_0^\pi \left| e^{-\jmath \overline{f}_m \cos\theta} - \mathbf{c}_N^H \mathbf{p}_{\mathrm{C}}\left(\cos\theta\right)\right|^2 d\theta\\
&= 1 - \mathbf{v}_{\mathrm{C}}^H\left(\jmath\overline{f}_m\right)\mathbf{c}_N - \mathbf{c}_N^H \mathbf{v}_{\mathrm{C}}\left(\jmath\overline{f}_m\right) + \mathbf{c}_N^H \mathbf{M}_{\mathrm{C}} \mathbf{c}_N,
\end{aligned}$$

where

$$\mathbf{c}_N = \begin{bmatrix} c_0 & c_1 & \cdots & c_N \end{bmatrix}^T,$$

$$\mathbf{v}_{\mathrm{C}}\left(\jmath\overline{f}_m\right) = \frac{1}{\pi}\int_0^{\pi} e^{\jmath\overline{f}_m\cos\theta}\mathbf{p}_{\mathrm{C}}\left(\cos\theta\right)d\theta,$$

$$\mathbf{M}_{\mathrm{C}} = \frac{1}{\pi}\int_0^{\pi} \mathbf{p}_{\mathrm{C}}\left(\cos\theta\right)\mathbf{p}_{\mathrm{C}}^T\left(\cos\theta\right)d\theta.$$

The minimization of the LSE criterion gives the optimal solution:

$$\mathbf{c}_N = \mathbf{M}_{\mathrm{C}}^{-1}\mathbf{v}_{\mathrm{C}}\left(\jmath\overline{f}_m\right). \tag{13}$$

Let us have a closer look at $\mathbf{v}_{\mathrm{C}}\left(\jmath\overline{f}_m\right)$ and $\mathbf{M}_{\mathrm{C}}$.

The elements of the vector $\mathbf{v}_{\mathrm{C}}\left(\jmath\overline{f}_m\right)$ are

$$\begin{aligned}\left[\mathbf{v}_{\mathrm{C}}\left(\jmath\overline{f}_m\right)\right]_{n+1} &= \frac{1}{\pi}\int_0^{\pi} e^{\jmath\overline{f}_m\cos\theta}\cos\left(n\theta\right)d\theta \\ &= I_n\left(\jmath\overline{f}_m\right) = \jmath^n J_n\left(\overline{f}_m\right),\end{aligned} \tag{14}$$

with $n = 0, 1, \ldots, N$, where

$$I_n(z) = \frac{1}{\pi} \int_0^{\pi} e^{z \cos\theta} \cos(n\theta)\, d\theta \tag{15}$$

is the integral representation of the modified Bessel function of the first kind [4] and

$$\begin{aligned} J_n(z) &= \frac{\jmath^{-n}}{\pi} \int_0^{\pi} e^{\jmath z \cos\theta} \cos(n\theta)\, d\theta \\ &= \jmath^{-n} I_n(\jmath z) \end{aligned} \tag{16}$$

is the integral representation of the Bessel function of the first kind [4].

The elements of the matrix $\mathbf{M}_{\mathrm{C}}$ are

$$[\mathbf{M}_{\mathrm{C}}]_{i+1,j+1} = \frac{1}{\pi} \int_0^{\pi} \cos(i\theta) \cos(j\theta)\, d\theta, \tag{17}$$

with $i, j = 0, 1, \ldots, N$.

It can be checked that

$$\begin{cases} [\mathbf{M}_{\mathrm{C}}]_{1,1} = 1, & \\ [\mathbf{M}_{\mathrm{C}}]_{i+1,i+1} = \dfrac{1}{2}, & i \geq 1 \\ [\mathbf{M}_{\mathrm{C}}]_{i+1,j+1} = 0, & i \neq j \end{cases} .$$

This is a consequence of the fact that Chebyshev polynomials are orthogonal.

Therefore, the matrix $\mathbf{M}_{\mathrm{C}}$ is diagonal, i.e.,

$$\mathbf{M}_{\mathrm{C}} = \mathrm{diag}\left(1, \frac{1}{2}, \ldots, \frac{1}{2}\right). \tag{18}$$

We deduce that the exponential function given in (11) can be expressed as [3]

$$e^{\jmath \overline{f}_m \cos\theta} = J_0\left(\overline{f}_m\right) + 2\sum_{n=1}^{\infty} \jmath^n J_n\left(\overline{f}_m\right)\cos\left(n\theta\right)$$
$$= \sum_{n=0}^{\infty} \jmath_n J_n\left(\overline{f}_m\right)\cos\left(n\theta\right), \tag{19}$$

where

$$\jmath_n = \begin{cases} 1, & n = 0 \\ 2\jmath^n, & n = 1, 2, \ldots, N \end{cases}.$$

Equation (19) is actually the well-known Jacobi-Anger expansion [6], [7], which represents an expansion of plane waves into a series of cylindrical waves.

Using (19) in the definition of the beampattern corresponding to $\mathbf{h}(f)$, we obtain

$$\begin{aligned}\mathcal{B}\left[\mathbf{h}(f),\cos\theta\right] &= \sum_{m=1}^{M} H_m(f) e^{\jmath \overline{f}_m \cos\theta} \\ &= \sum_{m=1}^{M} H_m(f) \sum_{n=0}^{\infty} \jmath_n J_n\left(\overline{f}_m\right)\cos\left(n\theta\right) \\ &= \sum_{n=0}^{\infty} \cos\left(n\theta\right)\left[\sum_{m=1}^{M} \jmath_n J_n\left(\overline{f}_m\right) H_m(f)\right]. \end{aligned} \tag{20}$$

If we limit the expansion to the order N, $\mathcal{B}\left[\mathbf{h}(f),\cos\theta\right]$ can be approximated by

$$\mathcal{B}_N\left[\mathbf{h}(f),\cos\theta\right] = \sum_{n=0}^{N} \cos\left(n\theta\right)\left[\sum_{m=1}^{M} \jmath_n J_n\left(\overline{f}_m\right) H_m(f)\right]. \tag{21}$$

For $m = 1$, $\overline{f}_1 = 0$, so that $J_0\left(\overline{f}_1\right) = 1$ and $J_n\left(\overline{f}_1\right) = 0,\ n = 1, 2, \ldots, N$.

We will see how to use (21) in order to design any desired symmetric beampattern or, equivalently, any desired DSA beampattern of any order.

Next, we explain different approaches.

Nonrobust Approach

In the nonrobust approach, it is always assumed that the number of sensors is equal to the order plus 1, i.e., $M = N + 1$.

This is how all DSA beampatterns have been traditionally designed [8], [9].

Because of this relation between the number of sensors and the DSA order, the white noise amplification problem gets much worse quicker as the order increases; in this sense, this technique is a nonrobust one.

The beampattern in (21) can be rewritten as

$$\mathcal{B}_{M-1}\left[\mathbf{h}(f), \cos\theta\right] = \sum_{i=0}^{M-1} \cos\left(i\theta\right) \overline{\mathbf{b}}_i^T(f)\mathbf{h}(f), \tag{22}$$

where $M \geq 2$ and

$$\overline{\mathbf{b}}_i(f) = \jmath_i \left[\begin{array}{cccc} J_i\left(\overline{f}_1\right) & J_i\left(\overline{f}_2\right) & \cdots & J_i\left(\overline{f}_M\right) \end{array} \right]^T. \tag{23}$$

In the proposed beampattern design, we would like to find the filter $\mathbf{h}(f)$ in such a way that $\mathcal{B}_{M-1}\left[\mathbf{h}(f), \cos\theta\right]$ is an $(M-1)$th-order frequency-invariant DSA beampattern, i.e.,

$$\mathcal{B}_{M-1}\left[\mathbf{h}(f), \cos\theta\right] = \mathcal{B}\left(\mathbf{b}_{M-1}, \cos\theta\right), \tag{24}$$

where $\mathcal{B}\left(\mathbf{b}_{M-1}, \cos\theta\right)$ is defined in (6).

By simple identification, we easily find that

$$\overline{\mathbf{B}}_{M-1}(f)\mathbf{h}(f) = \mathbf{b}_{M-1}, \tag{25}$$

where

$$\overline{\mathbf{B}}_{M-1}(f) = \begin{bmatrix} \overline{\mathbf{b}}_0^T(f) \\ \overline{\mathbf{b}}_1^T(f) \\ \vdots \\ \overline{\mathbf{b}}_{M-1}^T(f) \end{bmatrix} \tag{26}$$

is an $M \times M$ matrix.

Assuming that $\overline{\mathbf{B}}_{M-1}(f)$ is a full-rank matrix, we find that the nonrobust filter for beampattern design is

$$\mathbf{h}_{\mathrm{NR}}(f) = \overline{\mathbf{B}}_{M-1}^{-1}(f)\mathbf{b}_{M-1}. \tag{27}$$

Let us take the example of $M = 2$.

It is easy to check that

$$\mathcal{B}_1\left[\mathbf{h}(f),\cos\theta\right]=H_1(f)+J_0\left(\overline{f}_2\right)H_2(f)+2\jmath J_1\left(\overline{f}_2\right)H_2(f)\cos\theta, \tag{28}$$

$$\mathcal{B}\left(\mathbf{b}_1,\cos\theta\right)=b_{1,0}+b_{1,1}\cos\theta. \tag{29}$$

Identifying the two previous expressions, we get

$$H_{2,\mathrm{NR}}(f)=\frac{b_{1,1}}{2\jmath J_1\left(\overline{f}_2\right)} \tag{30}$$

and

$$H_{1,\mathrm{NR}}(f)=-J_0\left(\overline{f}_2\right)H_{2,\mathrm{NR}}(f)+b_{1,0}. \tag{31}$$

Therefore, with this approach, we can design any first-order DSA beampattern.

Depending on the values of $b_{1,0}$ and $b_{1,1}$ we find four interesting first-order DSAs.

- Dipole: $b_{1,0} = 0$ and $b_{1,1} = 1$.
- Cardioid: $b_{1,0} = \frac{1}{2}$ and $b_{1,1} = \frac{1}{2}$.
- Hypercardioid: $b_{1,0} = \frac{1}{4}$ and $b_{1,1} = \frac{3}{4}$.
- Supercardioid: $b_{1,0} = \frac{\sqrt{3}-1}{2}$ and $b_{1,1} = \frac{3-\sqrt{3}}{2}$.

Figure 1 displays the patterns [with $\mathbf{h}_{\mathrm{NR}}(f)$ defined in (27)] of the first-order dipole, cardioid, hypercardioid, and supercardioid for $f = 1$ kHz and $\delta = 0.5$ cm.

We observe that the designed patterns have less explicit nulls than the corresponding first-order directivity patterns.

This is due to the Jacobi-Anger series approximation.

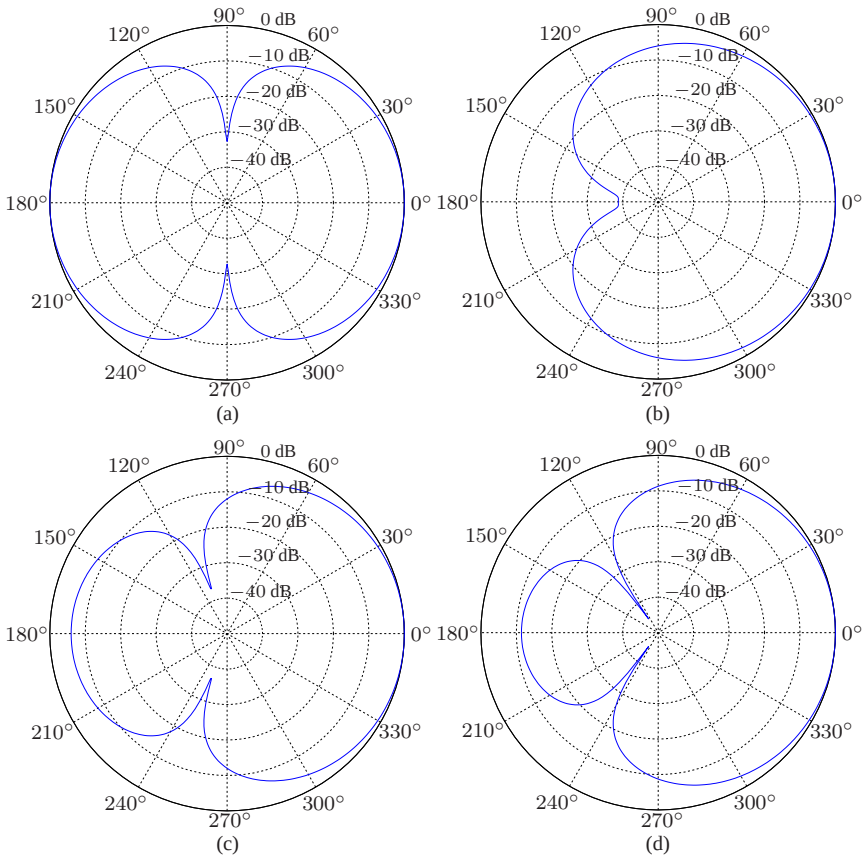

Figure 1: Beampatterns of the nonrobust first-order DSAs: (a) dipole, (b) cardioid, (c) hypercardioid, and (d) supercardioid. $M = 2$, $\delta = 0.5$ cm, and $f = 1$ kHz.

Figure 2 shows plots of the DF, $\mathcal{D}\left[\mathbf{h}_{\mathrm{NR}}(f)\right]$, as a function of frequency, for the dipole, cardioid, hypercardioid, and supercardioid, and several values of δ.

Corresponding plots of the WNG, $\mathcal{W}\left[\mathbf{h}_{\mathrm{NR}}(f)\right]$, as a function of frequency are depicted in Fig. 3.

We observe that for a small sensor spacing, the first-order DSAs give an approximately constant DF while the WNG is negative.

The white noise amplification is especially high at low frequencies. Increasing the sensor spacing enables to increase the WNG, but reduces the DF, especially at high frequencies.

A large value of δ is in contradiction with the DSA assumption, which results in deterioration of the beampatterns at high frequencies.

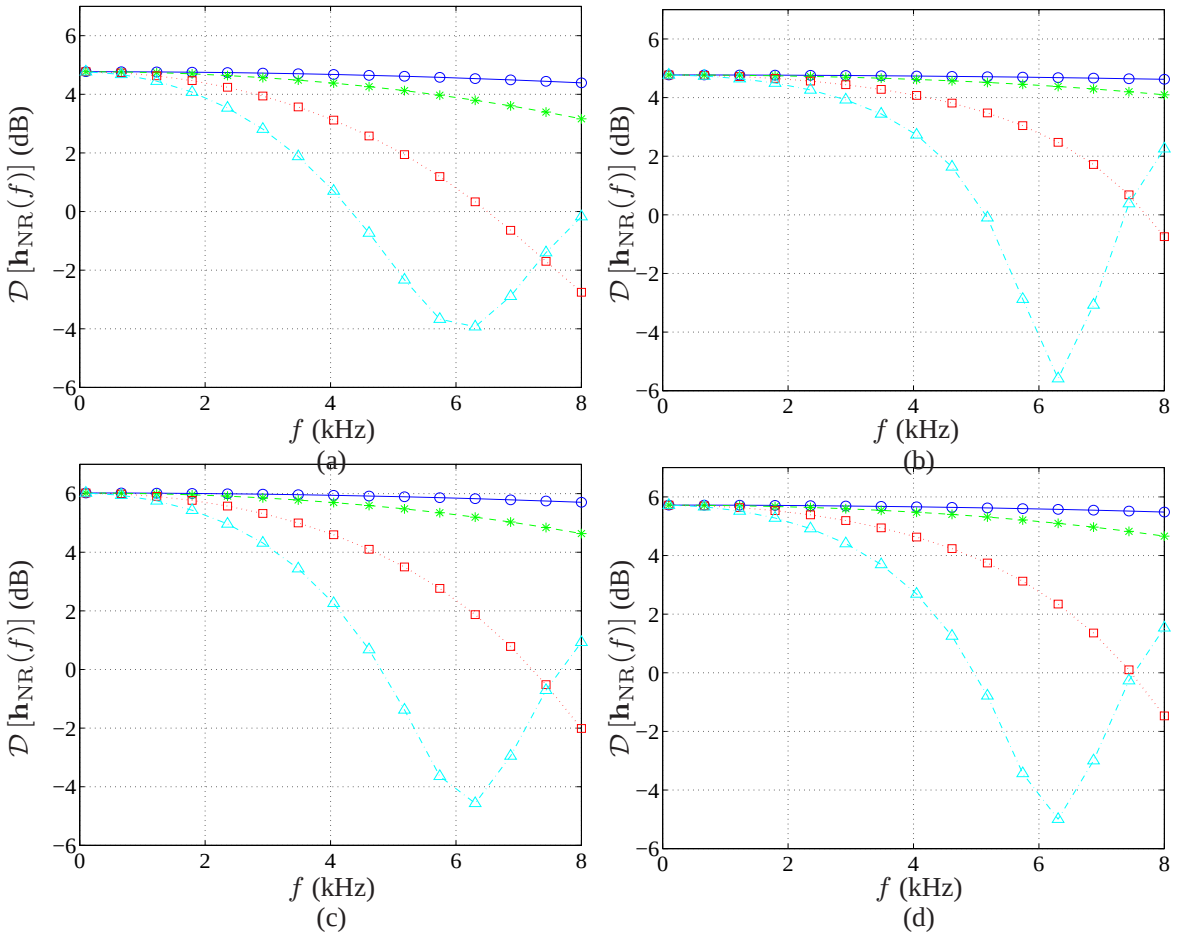

Figure 2: DF of the nonrobust first-order DSAs as a function of frequency, for $M = 2$ and several values of δ: $\delta = 0.1$ cm (solid line with circles), $\delta = 1$ cm (dashed line with asterisks), $\delta = 2$ cm (dotted line with squares), and $\delta = 3$ cm (dash-dot line with triangles). (a) Dipole, (b) cardioid, (c) hypercardioid, and (d) supercardioid.

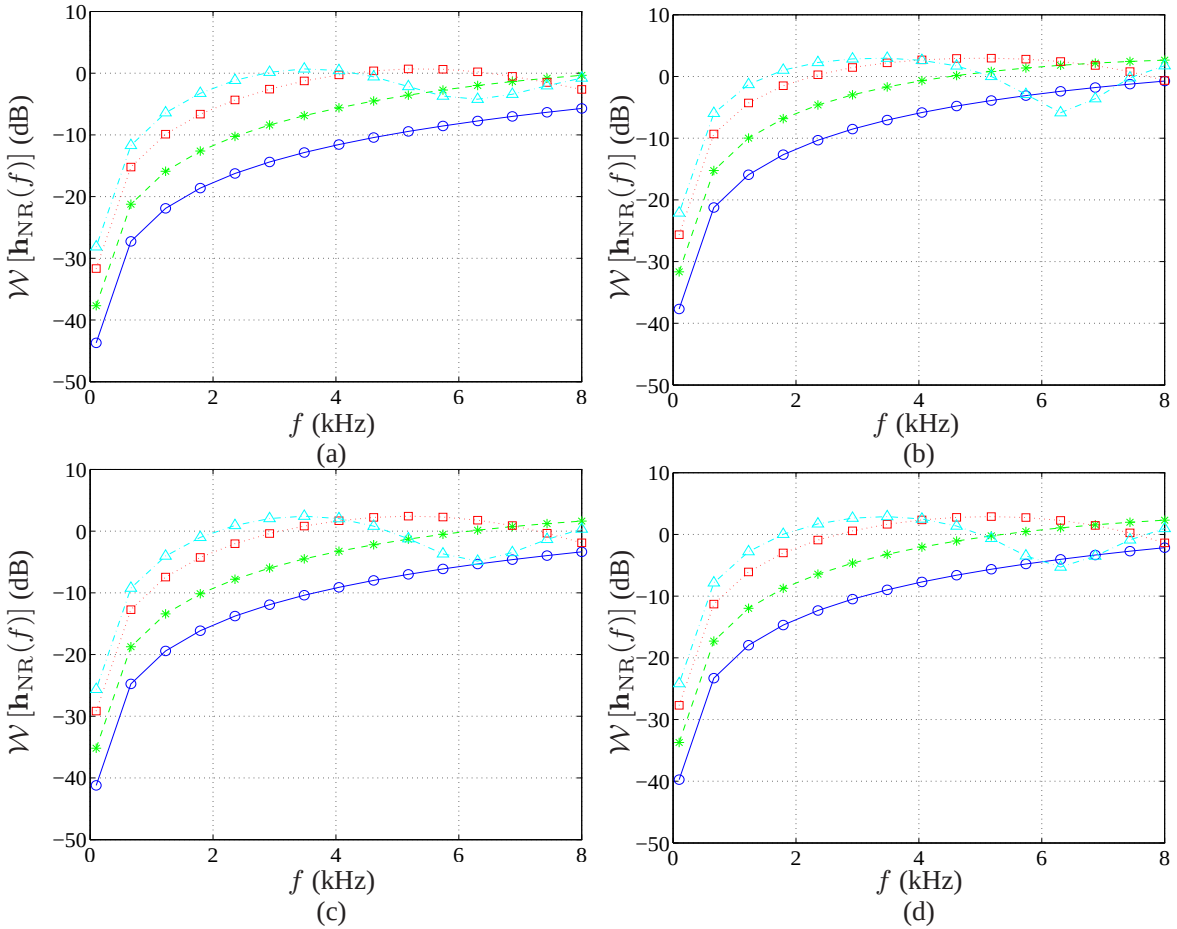

Figure 3: WNG of the nonrobust first-order DSAs as a function of frequency, for $M = 2$ and several values of δ: $\delta = 0.1$ cm (solid line with circles), $\delta = 1$ cm (dashed line with asterisks), $\delta = 2$ cm (dotted line with squares), and $\delta = 3$ cm (dash-dot line with triangles). (a) Dipole, (b) cardioid, (c) hypercardioid, and (d) supercardioid.

Robust Approach

In the robust scenario, the number of sensors is greater than the DSA order plus 1, i.e., $M > N + 1$.

By taking advantage of the fact that we have many more sensors than the order, we can control white noise amplification; in this sense, this technique is a robust one.

Again, we would like to find the filter $\mathbf{h}(f)$ in such a way that $\mathcal{B}_N\left[\mathbf{h}(f), \cos\theta\right]$ is an Nth-order frequency-invariant DSA beampattern, i.e.,

$$\mathcal{B}_N\left[\mathbf{h}(f), \cos\theta\right] = \mathcal{B}\left(\mathbf{b}_N, \cos\theta\right). \tag{32}$$

By simple identification, we easily find that

$$\overline{\mathbf{B}}_N(f)\mathbf{h}(f) = \mathbf{b}_N, \tag{33}$$

where

$$\overline{\mathbf{B}}_N(f) = \begin{bmatrix} \overline{\mathbf{b}}_0^T(f) \\ \overline{\mathbf{b}}_1^T(f) \\ \vdots \\ \overline{\mathbf{b}}_N^T(f) \end{bmatrix} \tag{34}$$

is now an $(N+1) \times M$ matrix.

Assuming that $\overline{\mathbf{B}}_N^H(f)$ is a full-column rank matrix and taking the minimum-norm solution of (33), we find that the robust filter for beampattern design is

$$\mathbf{h}_{\mathrm{R}}(f) = \overline{\mathbf{B}}_N^H(f) \left[\overline{\mathbf{B}}_N(f) \overline{\mathbf{B}}_N^H(f) \right]^{-1} \mathbf{b}_N. \tag{35}$$

Let us take the example of the first-order case (i.e., $N = 1$) with $M > 2$.

We still want to find the coefficients $H_m(f),\ m = 1, 2, \ldots, M$ in such a way that $\mathcal{B}_1\left[\mathbf{h}(f), \cos\theta\right] = \mathcal{B}_1\left(\mathbf{b}_1, \cos\theta\right)$.

It is not hard to get

$$\left[\begin{array}{cccc} J_1\left(\overline{f}_2\right) & J_1\left(\overline{f}_3\right) & \cdots & J_1\left(\overline{f}_M\right) \end{array}\right] \left[\begin{array}{c} H_2(f) \\ H_3(f) \\ \vdots \\ H_M(f) \end{array}\right] = \frac{b_{1,1}}{2\jmath} \tag{36}$$

and

$$H_1(f) + \sum_{i=2}^{M} J_0\left(\overline{f}_i\right) H_i(f) = b_{1,0}. \tag{37}$$

Taking the minimum-norm solution of (36), it is clear that the filter coefficients are as follows:

$$H_{i,\mathrm{R}}(f) = \frac{J_1\left(\overline{f}_i\right) b_{1,1}}{2\jmath \sum_{j=2}^{M} J_1^2\left(\overline{f}_j\right)}, \ i = 2, 3, \ldots, M \tag{38}$$

and

$$H_{1,\mathrm{R}}(f) = -\sum_{i=2}^{M} J_0\left(\overline{f}_i\right) H_{i,\mathrm{R}}(f) + b_{1,0}. \tag{39}$$

The robust filter, $\mathbf{h}_{\mathrm{R}}(f)$, whose components are given in (39) and (38), is the minimum-norm filter for the design of first-order DSA beampatterns.

The WNG with $\mathbf{h}_{\mathrm{R}}(f)$ should be much better than the one with $\mathbf{h}_{\mathrm{NR}}(f)$.

Figures 4–7 display the patterns [with $\mathbf{h}_{\mathrm{R}}(f)$ defined in (35)] of the first-order dipole, cardioid, hypercardioid, and supercardioid for $f = 1$ kHz, $\delta = 0.5$ cm, and several values of M.

Figure 8 shows plots of the DF, $\mathcal{D}\left[\mathbf{h}_{\mathrm{R}}(f)\right]$, as a function of frequency, for the dipole, cardioid, hypercardioid, and supercardioid, and several values of M.

Corresponding plots of the WNG, $\mathcal{W}\left[\mathbf{h}_{\mathrm{R}}(f)\right]$, as a function of frequency are depicted in Fig. 9.

We can see that the WNG is considerably improved as M increases, while the beampatterns and the DFs do not change much. It is clearly seen that the WNG with $\mathbf{h}_{\mathrm{R}}(f)$ is much better than the one with $\mathbf{h}_{\mathrm{NR}}(f)$.

The larger is the number of sensors, the more robust is the first-order DSA against white noise amplification.

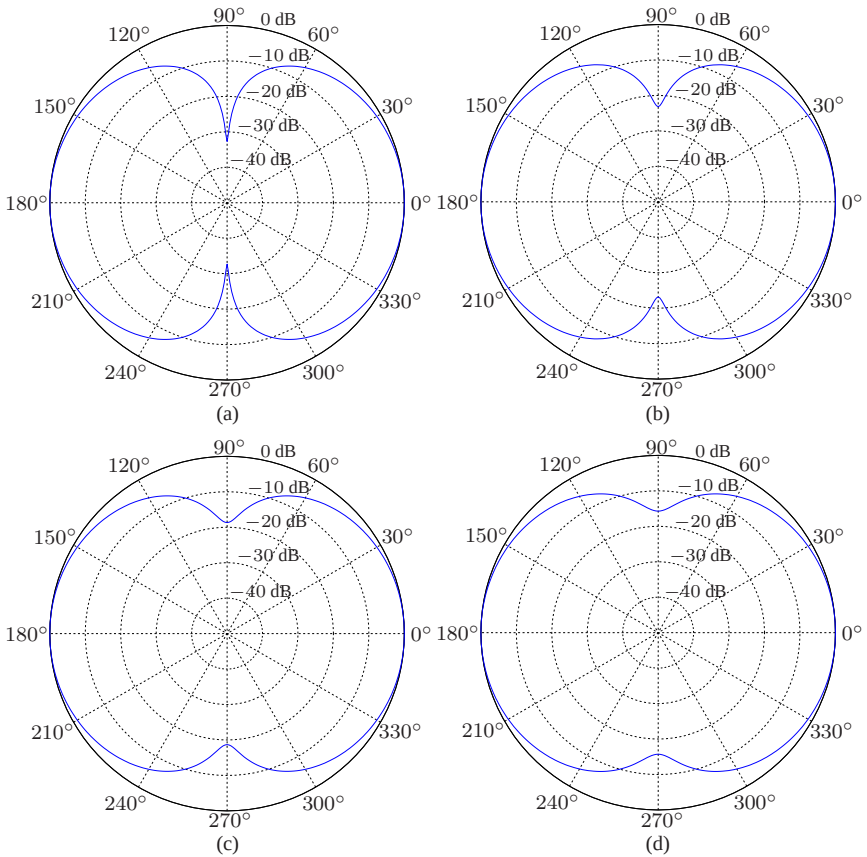

Figure 4: Beampatterns of the robust first-order dipole for $f = 1$ kHz, $\delta = 0.5$ cm, and several values of M: (a) $M = 2$, (b) $M = 4$, (c) $M = 6$, and (d) $M = 8$.

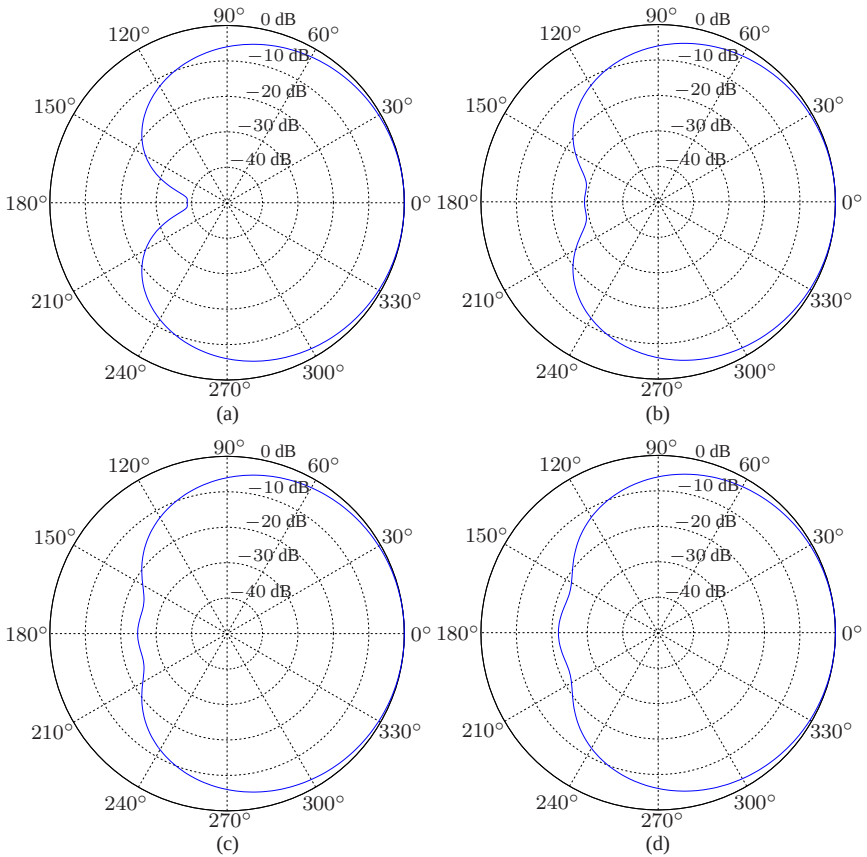

Figure 5: Beampatterns of the robust first-order cardioid for $f = 1$ kHz, $\delta = 0.5$ cm, and several values of M: (a) $M = 2$, (b) $M = 4$, (c) $M = 6$, and (d) $M = 8$.

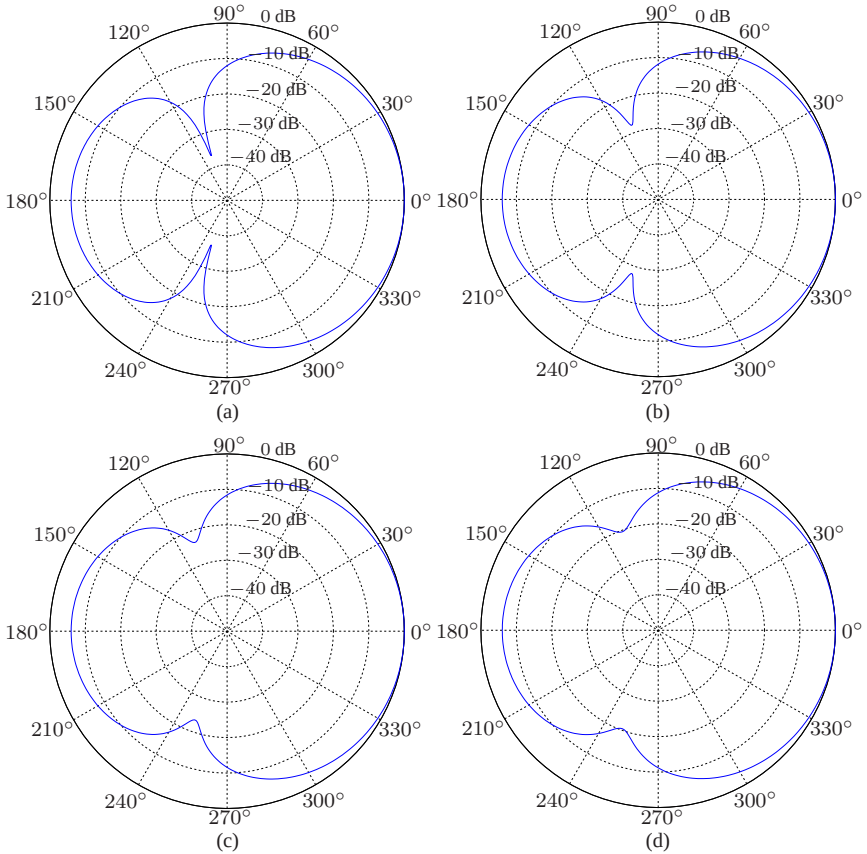

Figure 6: Beampatterns of the robust first-order hypercardioid for $f = 1$ kHz, $\delta = 0.5$ cm, and several values of M: (a) $M = 2$, (b) $M = 4$, (c) $M = 6$, and (d) $M = 8$.

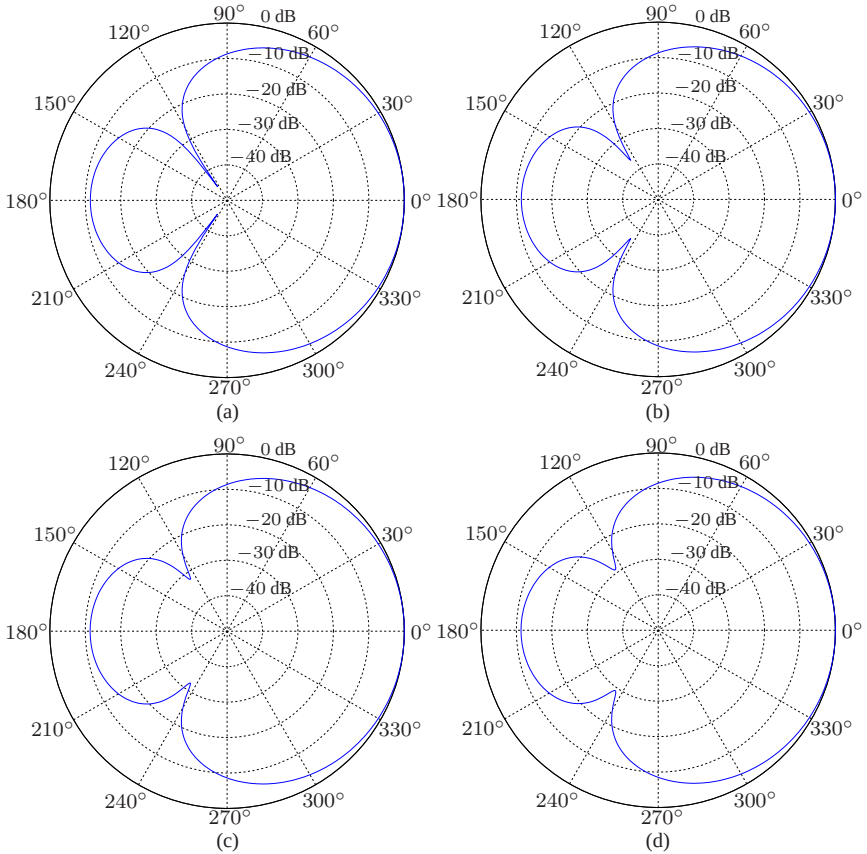

Figure 7: Beampatterns of the robust first-order supercardioid for $f = 1$ kHz, $\delta = 0.5$ cm, and several values of M: (a) $M = 2$, (b) $M = 4$, (c) $M = 6$, and (d) $M = 8$.

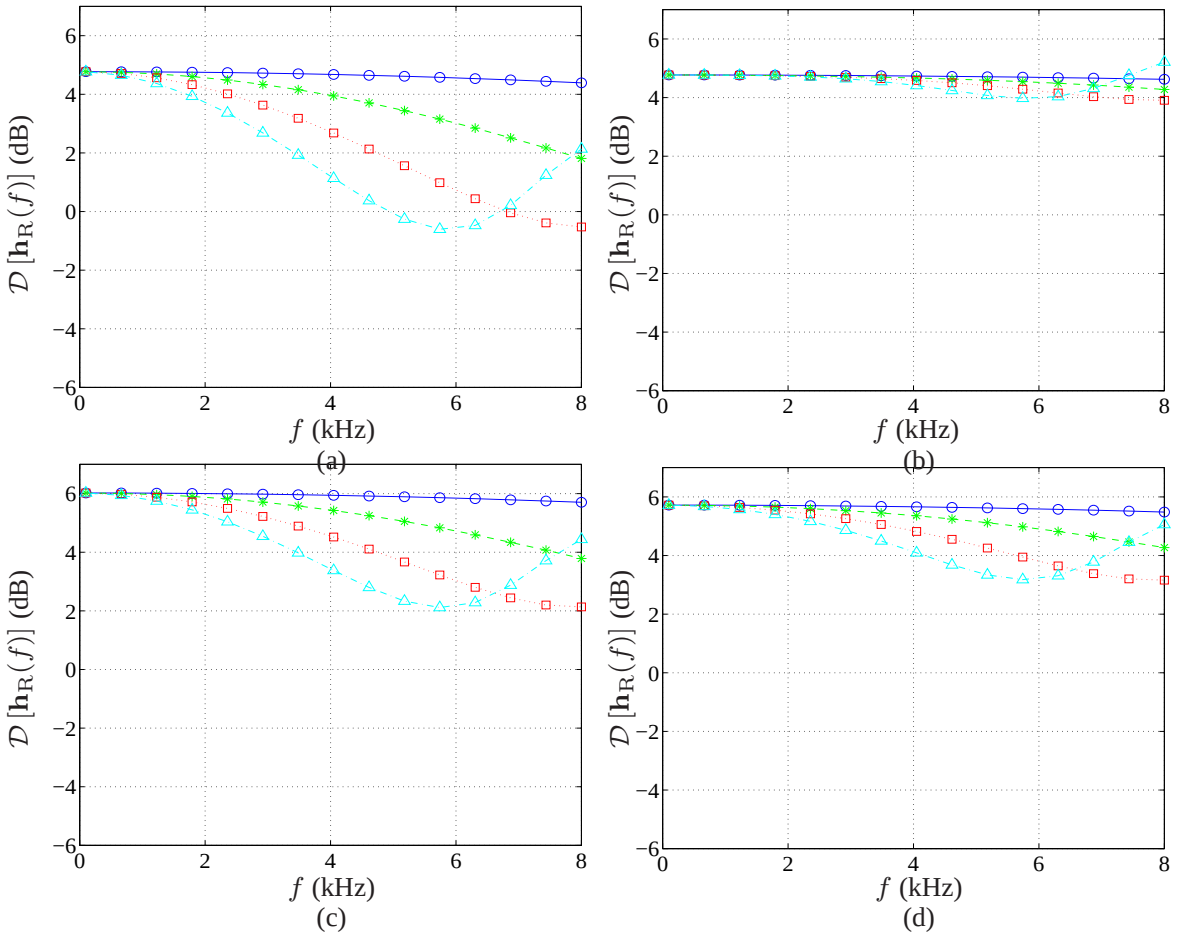

Figure 8: DF of the robust first-order DSAs as a function of frequency, for $\delta = 0.5$ cm and several values of M: $M = 2$ (solid line with circles), $M = 4$ (dashed line with asterisks), $M = 6$ (dotted line with squares), and $M = 8$ (dash-dot line with triangles). (a) Dipole, (b) cardioid, (c) hypercardioid, and (d) supercardioid.

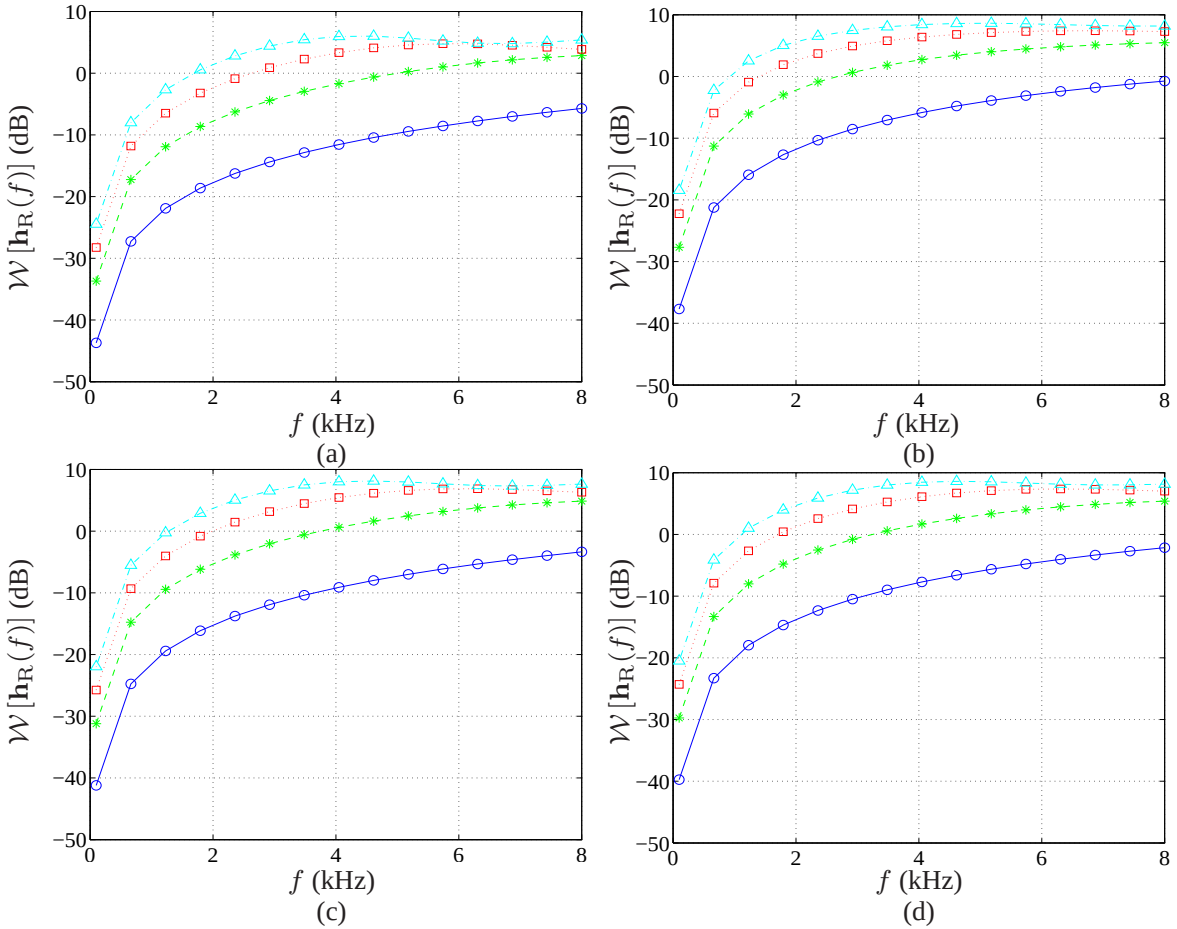

Figure 9: WNG of the robust first-order DSAs as a function of frequency, for $\delta = 0.5$ cm and several values of M: $M = 2$ (solid line with circles), $M = 4$ (dashed line with asterisks), $M = 6$ (dotted line with squares), and $M = 8$ (dash-dot line with triangles). (a) Dipole, (b) cardioid, (c) hypercardioid, and (d) supercardioid.

Frequency-Invariant Beampattern Design

Let us define the criterion:

$$J_{\mathrm{FI}}\left[\mathbf{h}(f)\right] = \frac{1}{\pi}\int_0^{\pi} \left|\mathcal{B}\left[\mathbf{h}(f), \cos\theta\right]\right|^2 d\theta \qquad (40)$$
$$= \mathbf{h}^H(f)\mathbf{\Gamma}_{\mathrm{C}}(f)\mathbf{h}(f),$$

where

$$\mathbf{\Gamma}_{\mathrm{C}}(f) = \frac{1}{\pi}\int_0^{\pi} \mathbf{d}\left(f, \cos\theta\right)\mathbf{d}^H\left(f, \cos\theta\right) d\theta. \qquad (41)$$

The (i,j)th (with $i, j = 1, 2, \ldots, M$) element of the $M \times M$ matrix $\mathbf{\Gamma}_{\mathrm{C}}(f)$ can be computed as

$$\left[\mathbf{\Gamma}_{\mathrm{C}}(f)\right]_{i,j} = \frac{1}{\pi}\int_0^{\pi} e^{\jmath 2\pi f(j-i)\tau_0 \cos\theta} d\theta \qquad (42)$$
$$= I_0\left[\jmath 2\pi f(j-i)\tau_0\right].$$

In order to design a frequency-invariant beampattern, we can minimize $J_{\mathrm{FI}}\left[\mathbf{h}(f)\right]$ subject to (33), i.e.,

$$\min_{\mathbf{h}(f)} \mathbf{h}^H(f)\mathbf{\Gamma}_{\mathrm{C}}(f)\mathbf{h}(f) \quad \text{subject to} \quad \overline{\mathbf{B}}_N(f)\mathbf{h}(f) = \mathbf{b}_N. \tag{43}$$

We easily find that the corresponding filter is

$$\mathbf{h}_{\mathrm{FI}}(f) = \mathbf{\Gamma}_{\mathrm{C}}^{-1}(f)\overline{\mathbf{B}}_N^H(f)\left[\overline{\mathbf{B}}_N(f)\mathbf{\Gamma}_{\mathrm{C}}^{-1}(f)\overline{\mathbf{B}}_N^H(f)\right]^{-1}\mathbf{b}_N. \tag{44}$$

When it comes to white noise amplification, the filter $\mathbf{h}_{\mathrm{FI}}(f)$ is usually much worse than the previous two derived filters $\mathbf{h}_{\mathrm{NR}}(f)$ and $\mathbf{h}_{\mathrm{R}}(f)$.

To better compromise with white noise amplification, we can use the following filter:

$$\mathbf{h}_{\mathrm{FI},\epsilon}(f) = \mathbf{\Gamma}_{\mathrm{C},\epsilon}^{-1}(f)\overline{\mathbf{B}}_N^H(f)\left[\overline{\mathbf{B}}_N(f)\mathbf{\Gamma}_{\mathrm{C},\epsilon}^{-1}(f)\overline{\mathbf{B}}_N^H(f)\right]^{-1}\mathbf{b}_N, \tag{45}$$

where

$$\mathbf{\Gamma}_{\mathrm{C},\epsilon}(f) = \mathbf{\Gamma}_{\mathrm{C}}(f) + \epsilon \mathbf{I}_M, \tag{46}$$

with $\epsilon \geq 0$ being the regularization parameter.

It is clear that $\mathbf{h}_{\mathrm{FI},0}(f) = \mathbf{h}_{\mathrm{FI}}(f)$ and $\mathbf{h}_{\mathrm{FI},\infty}(f) = \mathbf{h}_{\mathrm{R}}(f)$.

Figures 10–13 display the patterns [with $\mathbf{h}_{\mathrm{FI},\epsilon}(f)$ defined in (45)] of the first-order dipole, cardioid, hypercardioid, and supercardioid for $f = 1$ kHz, $\delta = 0.5$ cm, $M = 6$, and several values of ϵ.

Figure 14 shows plots of the DF, $\mathcal{D}\left[\mathbf{h}_{\mathrm{FI},\epsilon}(f)\right]$, as a function of frequency, for the dipole, cardioid, hypercardioid, and supercardioid, and several values of ϵ.

Corresponding plots of the WNG, $\mathcal{W}\left[\mathbf{h}_{\mathrm{FI},\epsilon}(f)\right]$, as a function of frequency are depicted in Fig. 15.

We can see that the WNG is considerably improved as ϵ increases, while the beampatterns and the DFs do not change much.

The larger is ϵ, the more robust is the frequency-invariant first-order DSA against white noise amplification, but at the expense of less explicit nulls.

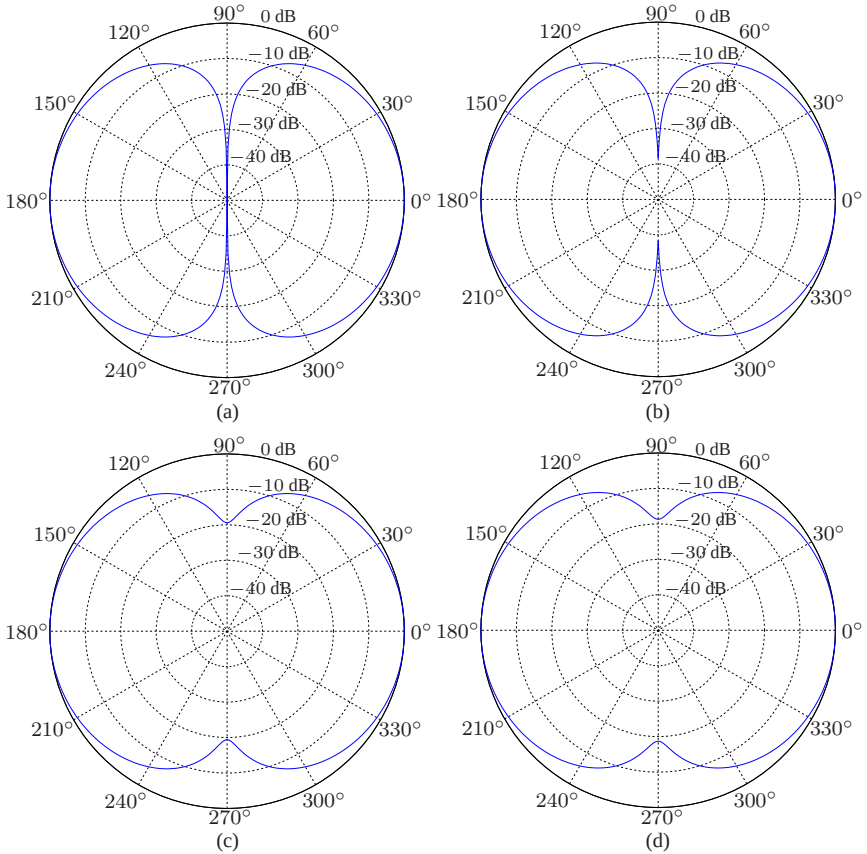

Figure 10: Beampatterns of the frequency-invariant first-order dipole for $f = 1$ kHz, $\delta = 0.5$ cm, $M = 6$, and several values of ϵ: (a) $\epsilon = 0$, (b) $\epsilon = 10^{-5}$, (c) $\epsilon = 10^{-3}$, and (d) $\epsilon = 0.1$.

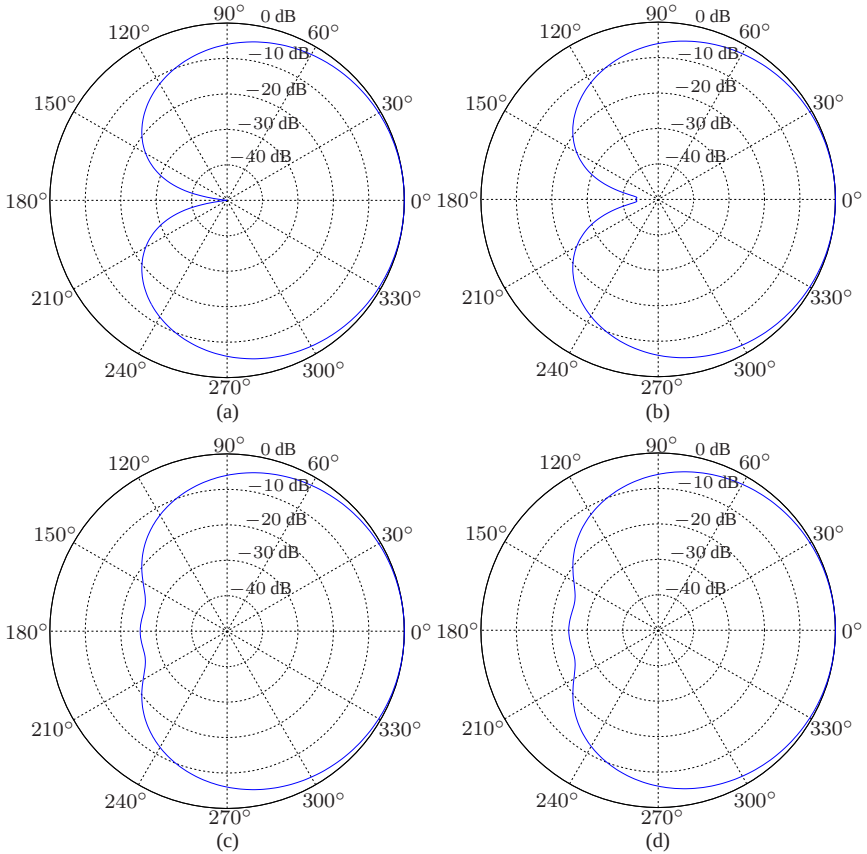

Figure 11: Beampatterns of the frequency-invariant first-order cardioid for $f = 1$ kHz, $\delta = 0.5$ cm, $M = 6$, and several values of ϵ: (a) $\epsilon = 0$, (b) $\epsilon = 10^{-5}$, (c) $\epsilon = 10^{-3}$, and (d) $\epsilon = 0.1$.

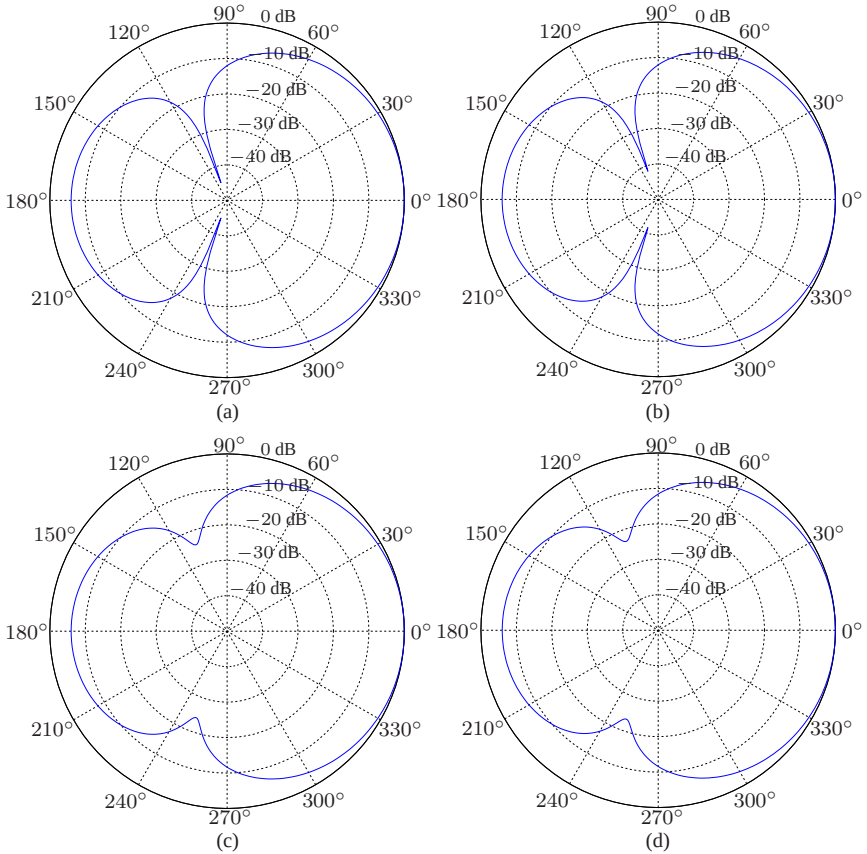

Figure 12: Beampatterns of the frequency-invariant first-order hypercardioid for $f = 1$ kHz, $\delta = 0.5$ cm, $M = 6$, and several values of ϵ: (a) $\epsilon = 0$, (b) $\epsilon = 10^{-5}$, (c) $\epsilon = 10^{-3}$, and (d) $\epsilon = 0.1$.

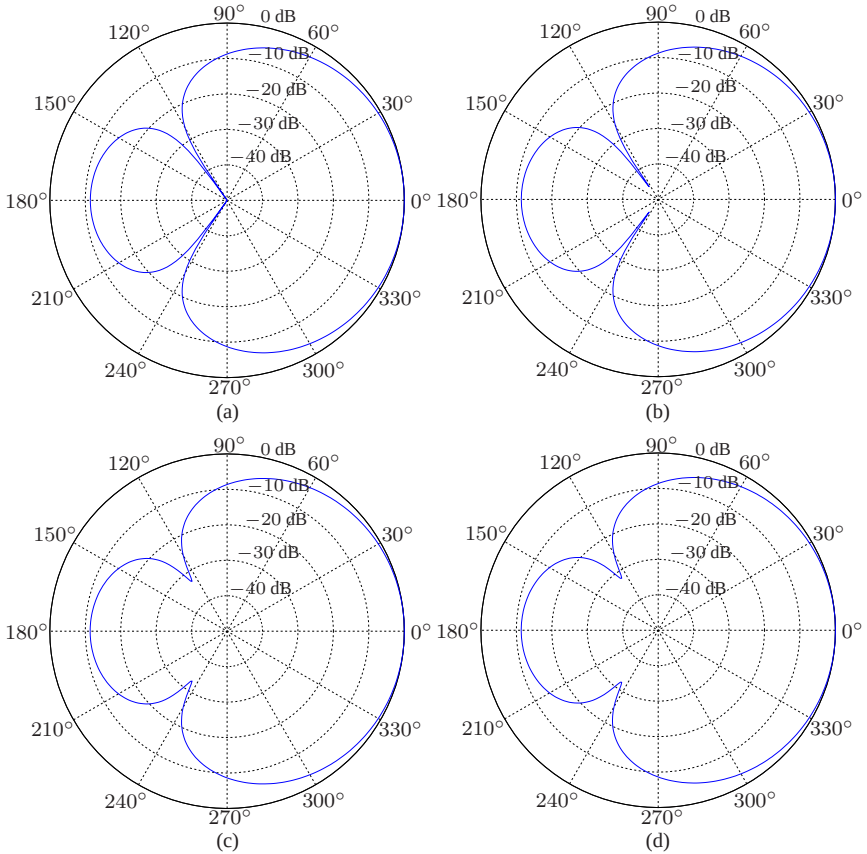

Figure 13: Beampatterns of the frequency-invariant first-order supercardioid for $f = 1$ kHz, $\delta = 0.5$ cm, $M = 6$, and several values of ϵ: (a) $\epsilon = 0$, (b) $\epsilon = 10^{-5}$, (c) $\epsilon = 10^{-3}$, and (d) $\epsilon = 0.1$.

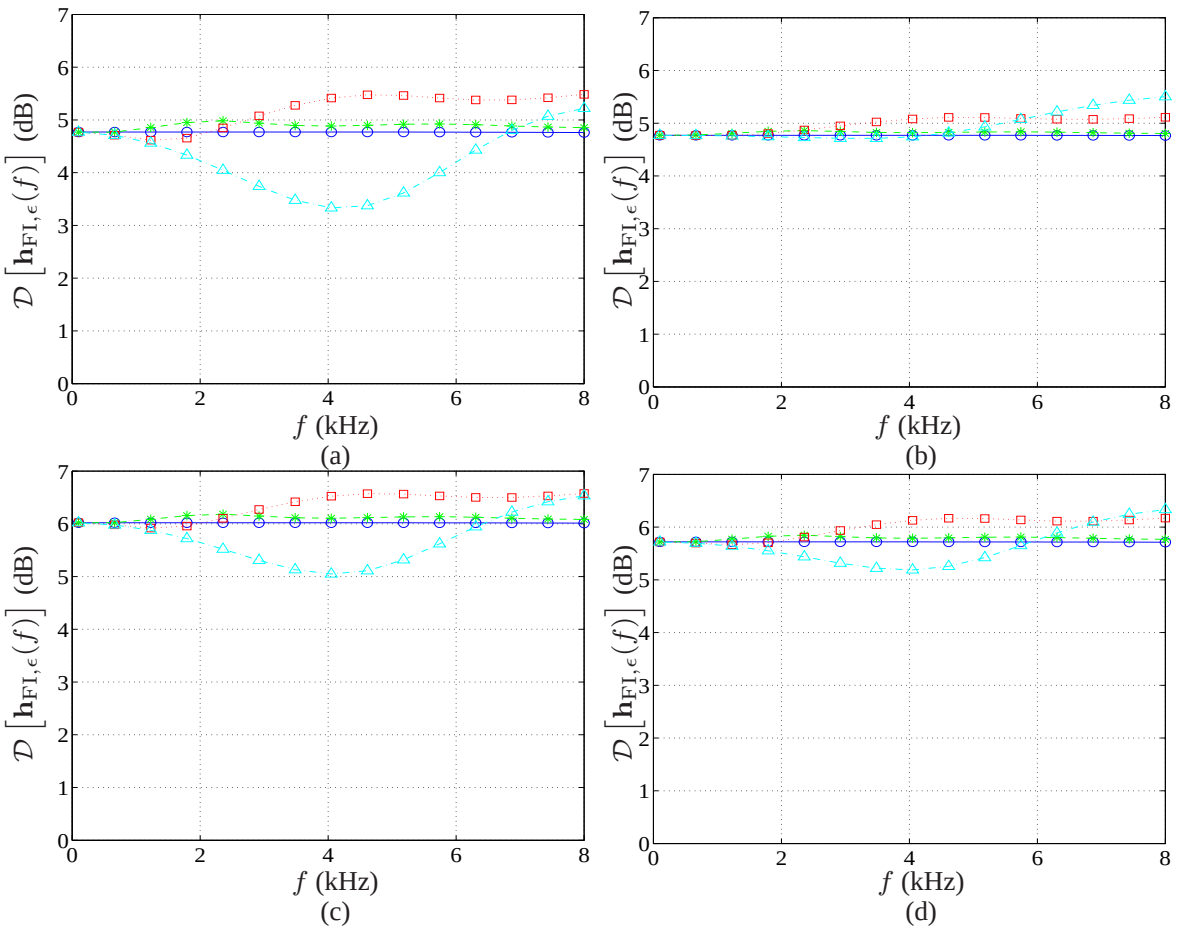

Figure 14: DF of the frequency-invariant first-order DSAs as a function of frequency, for $\delta = 0.5$ cm, $M = 6$, and several values of ϵ: $\epsilon = 0$ (solid line with circles), $\epsilon = 10^{-5}$ (dashed line with asterisks), $\epsilon = 10^{-3}$ (dotted line with squares), and $\epsilon = 0.1$ (dash-dot line with triangles). (a) Dipole, (b) cardioid, (c) hypercardioid, and (d) supercardioid.

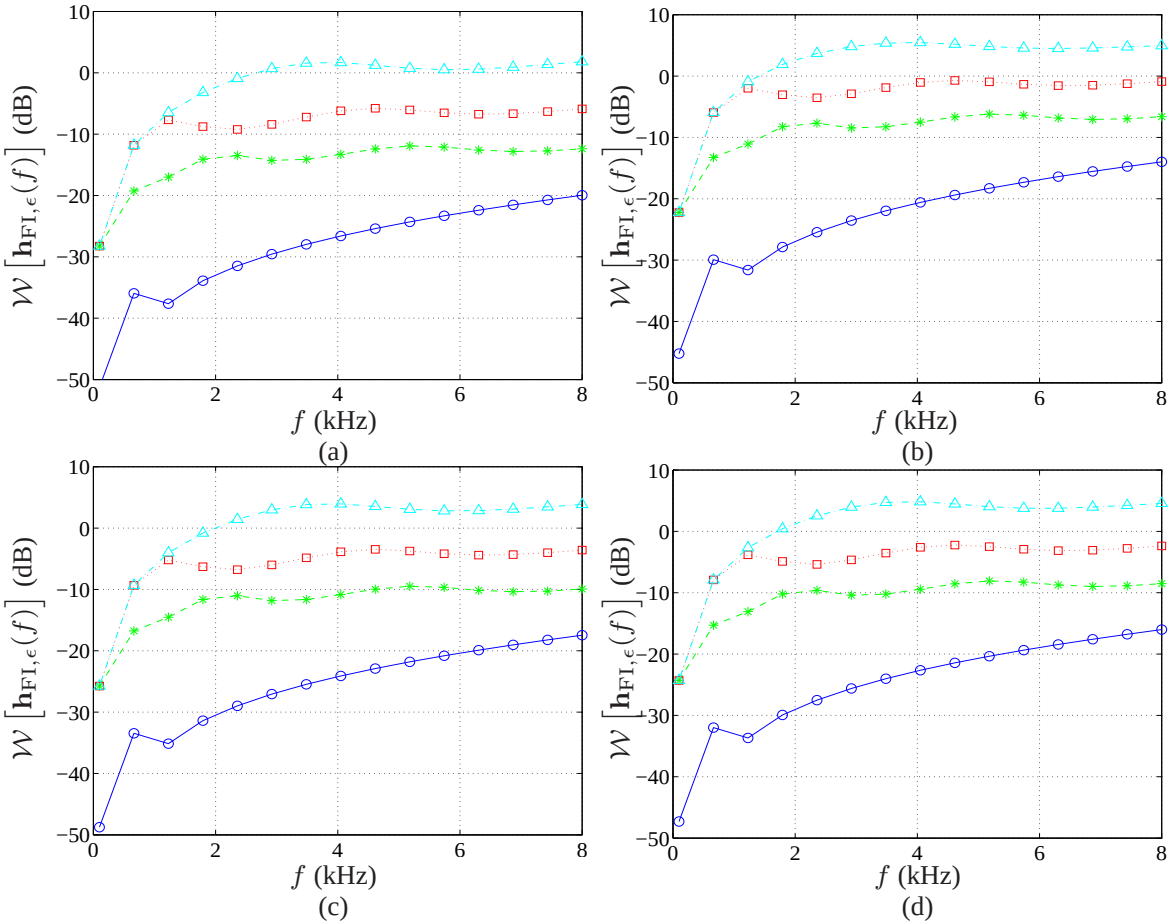

Figure 15: WNG of the frequency-invariant first-order DSAs as a function of frequency, for $\delta = 0.5$ cm, $M = 6$, and several values of ϵ: $\epsilon = 0$ (solid line with circles), $\epsilon = 10^{-5}$ (dashed line with asterisks), $\epsilon = 10^{-3}$ (dotted line with squares), and $\epsilon = 0.1$ (dash-dot line with triangles). (a) Dipole, (b) cardioid, (c) hypercardioid, and (d) supercardioid.

Least-Squares Method

Let us define the error signal between the array beampattern and the desired directivity pattern:

$$\begin{aligned}\mathcal{E}\left[\mathbf{h}(f),\cos\theta\right] &= \mathcal{B}\left[\mathbf{h}(f),\cos\theta\right]-\mathcal{B}\left(\mathbf{b}_N,\cos\theta\right) \\ &= \mathbf{d}^H\left(f,\cos\theta\right)\mathbf{h}(f)-\mathbf{p}_{\mathrm{C}}^T\left(\cos\theta\right)\mathbf{b}_N.\end{aligned} \tag{47}$$

Then, the least-squares (LS) method consists of minimizing the LSE:

$$\begin{aligned}\mathrm{LSE}\left[\mathbf{h}(f)\right] &= \frac{1}{\pi}\int_0^{\pi}\left|\mathcal{E}\left[\mathbf{h}(f),\cos\theta\right]\right|^2 d\theta \\ &= \mathbf{h}^H(f)\mathbf{\Gamma}_{\mathrm{C}}(f)\mathbf{h}(f)-\mathbf{h}^H(f)\mathbf{\Gamma}_{\mathbf{dp}_{\mathrm{C}}}(f)\mathbf{b}_N- \\ &\quad \mathbf{b}_N^T\mathbf{\Gamma}_{\mathbf{dp}_{\mathrm{C}}}^H(f)\mathbf{h}(f)+\mathbf{b}_N^T\mathbf{M}_{\mathrm{C}}\mathbf{b}_N,\end{aligned} \tag{48}$$

where

$$\mathbf{\Gamma}_{\mathbf{dp}_{\mathrm{C}}}(f)=\frac{1}{\pi}\int_0^{\pi}\mathbf{d}\left(f,\cos\theta\right)\mathbf{p}_{\mathrm{C}}^T\left(\cos\theta\right)d\theta, \tag{49}$$

and $\mathbf{\Gamma}_{\mathrm{C}}(f)$ and $\mathbf{M}_{\mathrm{C}}$ are defined in (41) and (18), respectively.

The minimization of (48) gives the LS filter:

$$\mathbf{h}_{\mathrm{LS}}(f) = \mathbf{\Gamma}_{\mathrm{C}}^{-1}(f)\mathbf{\Gamma}_{\mathbf{dp}_{\mathrm{C}}}(f)\mathbf{b}_N. \tag{50}$$

It is also easy to find the regularized LS filter:

$$\mathbf{h}_{\mathrm{LS},\epsilon}(f) = \mathbf{\Gamma}_{\mathrm{C},\epsilon}^{-1}(f)\mathbf{\Gamma}_{\mathbf{dp}_{\mathrm{C}}}(f)\mathbf{b}_N. \tag{51}$$

Another more interesting idea is to minimize the LSE criterion subject to the distortionless constraint [2], i.e.,

$$\min_{\mathbf{h}(f)} \mathrm{LSE}\left[\mathbf{h}(f)\right] \quad \text{subject to} \quad \mathbf{h}^H(f)\mathbf{d}\left(f,1\right) = 1. \tag{52}$$

We easily obtain the constrained LS (CLS) filter:

$$\mathbf{h}_{\mathrm{CLS}}(f) = \mathbf{h}_{\mathrm{LS}}(f) - \frac{1 - \mathbf{d}^H\left(f,1\right)\mathbf{h}_{\mathrm{LS}}(f)}{\mathbf{d}^H\left(f,1\right)\mathbf{\Gamma}_{\mathrm{C}}^{-1}(f)\mathbf{d}\left(f,1\right)}\mathbf{\Gamma}_{\mathrm{C}}^{-1}(f)\mathbf{d}\left(f,1\right). \tag{53}$$

A more robust version is the regularized CLS filter:

$$\mathbf{h}_{\mathrm{CLS},\epsilon}(f) = \mathbf{h}_{\mathrm{LS},\epsilon}(f) - \frac{1 - \mathbf{d}^H(f,1)\,\mathbf{h}_{\mathrm{LS},\epsilon}(f)}{\mathbf{d}^H(f,1)\,\boldsymbol{\Gamma}_{\mathrm{C},\epsilon}^{-1}(f)\mathbf{d}(f,1)}\boldsymbol{\Gamma}_{\mathrm{C},\epsilon}^{-1}(f)\mathbf{d}(f,1)\,. \quad (54)$$

The error signal defined in (47) can also be expressed as

$$\begin{aligned}\mathcal{E}\left[\mathbf{h}(f), \cos\theta\right] &= \sum_{i=0}^{\infty} \cos(i\theta)\,\overline{\mathbf{b}}_i^T(f)\mathbf{h}(f) - \sum_{i=0}^{N} b_{N,i}\cos(i\theta) \quad (55)\\ &= \sum_{i=0}^{N} \cos(i\theta)\,\overline{\mathbf{b}}_i^T(f)\mathbf{h}(f) - \sum_{i=0}^{N} b_{N,i}\cos(i\theta) + \\ &\quad \sum_{i=N+1}^{\infty} \cos(i\theta)\,\overline{\mathbf{b}}_i^T(f)\mathbf{h}(f).\end{aligned}$$

Using the constraint $\overline{\mathbf{B}}_N(f)\mathbf{h}(f) = \mathbf{b}_N$ [or, equivalently, $\overline{\mathbf{b}}_i^T(f)\mathbf{h}(f) = b_{N,i},\ i = 0, 1, \ldots, N$] in the first element on the right-hand side of the previous expression, the error simplifies to

$$\mathcal{E}\left[\mathbf{h}(f), \cos\theta\right] = \sum_{i=N+1}^{\infty} \cos\left(i\theta\right) \overline{\mathbf{b}}_i^T(f)\mathbf{h}(f). \tag{56}$$

Therefore, the (constrained) LSE criterion is also

$$\mathrm{LSE}\left[\mathbf{h}(f)\right] = \frac{1}{\pi}\int_0^{\pi} \left| \sum_{i=N+1}^{\infty} \cos\left(i\theta\right) \overline{\mathbf{b}}_i^T(f)\mathbf{h}(f) \right|^2 d\theta. \tag{57}$$

Using (56), the criterion defined in (40) can be expressed as

$$J_{\mathrm{FI}}\left[\mathbf{h}(f)\right] = \frac{1}{\pi}\int_0^{\pi} \left|\mathcal{E}\left[\mathbf{h}(f), \cos\theta\right] + \mathcal{B}\left(\mathbf{b}_N, \cos\theta\right)\right|^2 d\theta \tag{58}$$

$$= \frac{1}{\pi}\int_0^{\pi} \left|\sum_{i=N+1}^{\infty} \cos\left(i\theta\right) \overline{\mathbf{b}}_i^T(f)\mathbf{h}(f) + \sum_{i=0}^{N} b_{N,i}\cos\left(i\theta\right)\right|^2 d\theta.$$

Using the orthogonality property of the Chebyshev polynomials, the previous expression simplifies to

$$J_{\mathrm{FI}}\left[\mathbf{h}(f)\right] = \mathrm{LSE}\left[\mathbf{h}(f)\right] + \frac{1}{\pi}\int_0^{\pi} \left|\mathcal{B}\left(\mathbf{b}_N, \cos\theta\right)\right|^2 d\theta, \tag{59}$$

where the second term on the right-hand side of (59) does not depend on $\mathbf{h}(f)$.

This shows that minimizing $J_{\mathrm{FI}}\left[\mathbf{h}(f)\right]$ subject to the constraint $\overline{\mathbf{B}}_N(f)\mathbf{h}(f) = \mathbf{b}_N$ is equivalent to minimizing $\mathrm{LSE}\left[\mathbf{h}(f)\right]$ subject to the same constraint.

Figures 16 displays the patterns [with $\mathbf{h}_{\mathrm{LS},\epsilon}(f)$ defined in (51)] of the first-order supercardioid for $f = 1$ kHz, $\delta = 0.5$ cm, $M = 6$, and several values of ϵ.

Corresponding plots of the first-order supercardioid, obtained with $\mathbf{h}_{\mathrm{CLS},\epsilon}(f)$ [defined in (54)] are depicted in Fig. 17.

Figure 18 shows plots of the DFs, $\mathcal{D}\left[\mathbf{h}_{\mathrm{LS},\epsilon}(f)\right]$ and $\mathcal{D}\left[\mathbf{h}_{\mathrm{CLS},\epsilon}(f)\right]$, as a function of frequency, for the first-order supercardioid and several values of ϵ.

Corresponding plots of the WNGs, $\mathcal{W}\left[\mathbf{h}_{\mathrm{LS},\epsilon}(f)\right]$ and $\mathcal{W}\left[\mathbf{h}_{\mathrm{CLS},\epsilon}(f)\right]$, as a function of frequency are depicted in Fig. 19.

We observe that the WNG is considerably improved as ϵ increases, while the beampatterns and the DFs do not change much as long as ϵ is not too large.

The larger is ϵ, the more robust are the regularized LS and CLS first-order DSAs against white noise amplification, but at the expense of less explicit nulls.

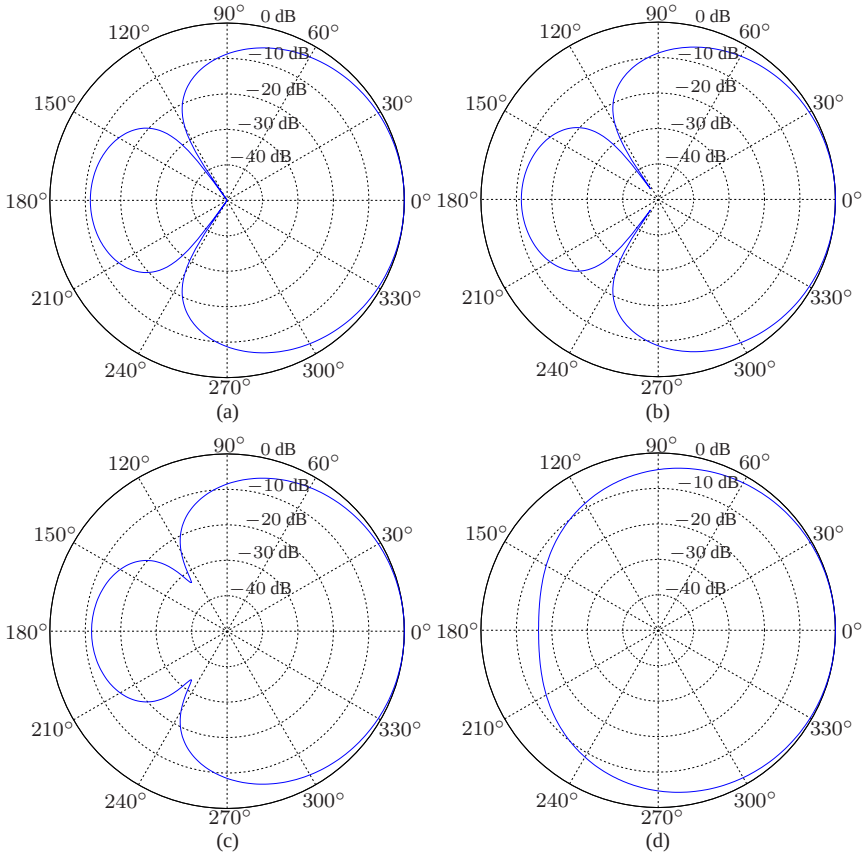

Figure 16: Beampatterns of the regularized LS first-order supercardioid for $f = 1$ kHz, $\delta = 0.5$ cm, $M = 6$, and several values of ϵ: (a) $\epsilon = 0$, (b) $\epsilon = 10^{-5}$, (c) $\epsilon = 10^{-3}$, and (d) $\epsilon = 0.1$.

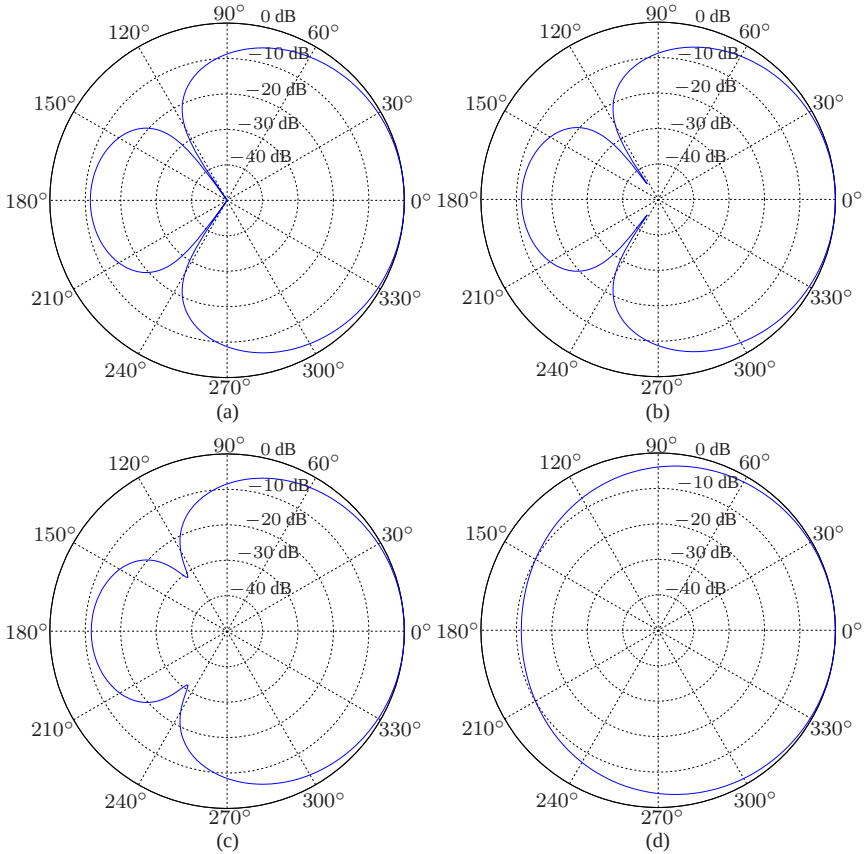

Figure 17: Beampatterns of the regularized CLS first-order supercardioid for $f = 1$ kHz, $\delta = 0.5$ cm, $M = 6$, and several values of ϵ: (a) $\epsilon = 0$, (b) $\epsilon = 10^{-5}$, (c) $\epsilon = 10^{-3}$, and (d) $\epsilon = 0.1$.

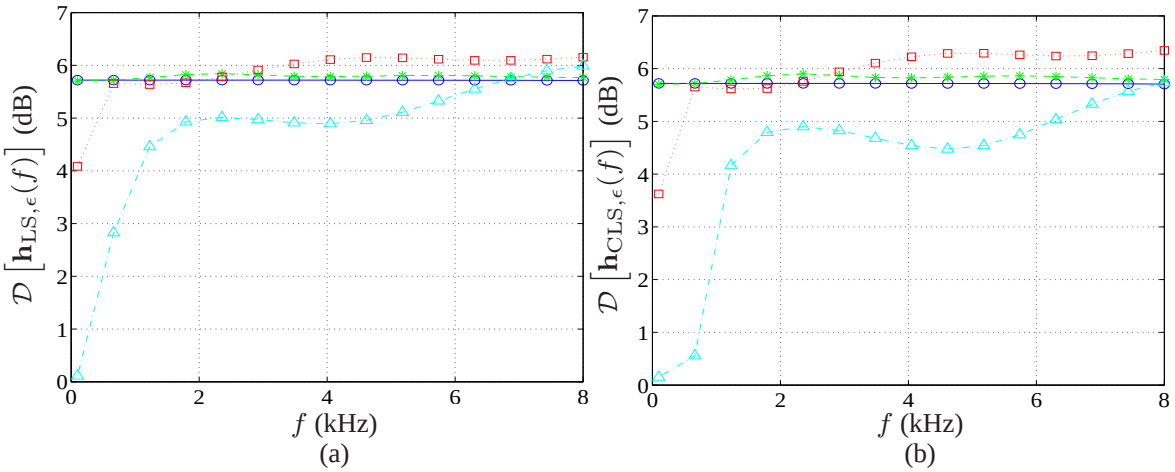

Figure 18: DF of first-order supercardioids as a function of frequency, for $\delta = 0.5$ cm, $M = 6$, and several values of ϵ: $\epsilon = 0$ (solid line with circles), $\epsilon = 10^{-5}$ (dashed line with asterisks), $\epsilon = 10^{-3}$ (dotted line with squares), and $\epsilon = 0.1$ (dash-dot line with triangles). (a) Regularized LS and (b) regularized CLS.

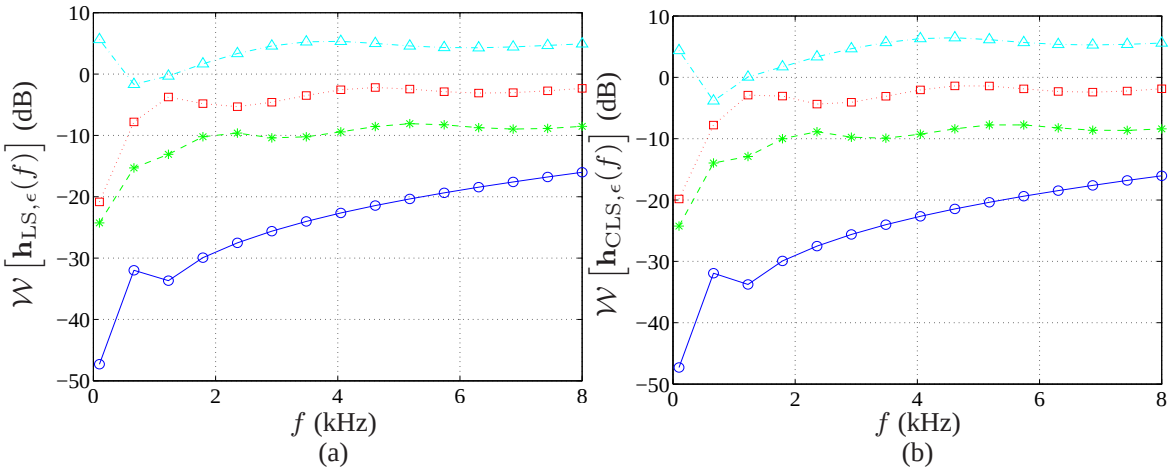

Figure 19: WNG of first-order supercardioids as a function of frequency, for $\delta = 0.5$ cm, $M = 6$, and several values of ϵ: $\epsilon = 0$ (solid line with circles), $\epsilon = 10^{-5}$ (dashed line with asterisks), $\epsilon = 10^{-3}$ (dotted line with squares), and $\epsilon = 0.1$ (dash-dot line with triangles). (a) Regularized LS and (b) regularized CLS.

Joint Optimization

Maximum WNG Filter

Here, of course, we assume that $M > N + 1$.

This gives us much more flexibility to design beampatterns with different compromises thanks to the array redundancy.

We denote by $\mathbf{h}'(f)$, the filter of length $N + 1$, which is equal to the filter $\mathbf{h}_{\mathrm{NR}}(f)$ with $N + 1 = M$.

In the rest, we are interested in the class of filters, of length $M (> N + 1)$, whose form is

$$\mathbf{h}(f) = \mathbf{H}'(f)\mathbf{g}(f), \tag{60}$$

where $\mathbf{H}'(f)$ is a matrix of size $M \times (M-N)$, with

$$\mathbf{H}'^H(f) = \begin{bmatrix} \mathbf{h}'^H(f) & & \mathbf{0}_{1\times(M-N-1)} \\ 0 & \mathbf{h}'^H(f) & \mathbf{0}_{1\times(M-N-2)} \\ \vdots & \ddots & \\ \mathbf{0}_{1\times(M-N-1)} & & \mathbf{h}'^H(f) \end{bmatrix}, \tag{61}$$

$\mathbf{h}'(f) = \mathbf{h}_{\mathrm{NR}}(f)$, and $\mathbf{g}(f) \neq \mathbf{0}$ is a filter of length $M-N$.

The fundamental property of the class of filters defined in (60) is that they preserve the nulls of $\mathbf{h}'(f) = \mathbf{h}_{\mathrm{NR}}(f)$.

Indeed, if θ_0 is a null of $\mathbf{h}'(f)$, it can be verified that, thanks to the structure of the steering vector, we have

$$\mathbf{h}^H(f)\mathbf{d}\left(f, \cos\theta_0\right) = \mathbf{g}^H(f)\widetilde{\mathbf{d}}\left(f, \cos\theta_0\right) \times 0 = 0, \tag{62}$$

where

$$\widetilde{\mathbf{d}}\left(f,\cos\theta_0\right)=\left[\begin{array}{cccc}1 & e^{-\jmath 2\pi f\tau_0\cos\theta_0} & \cdots & e^{-\jmath(M-N-1)2\pi f\tau_0\cos\theta_0}\end{array}\right]^T. \tag{63}$$

At this point, it is important to mention that what characterize and identify the different array beampatterns are their nulls in the different directions; so when the nulls are preserved, the shape of the beampatterns is also mostly preserved.

Now, we can play on the filter $\mathbf{g}(f)$ and its dimension to improve the WNG and/or the frequency invariance of the beampatterns.

At $\theta=0$, we have

$$\begin{aligned}\mathbf{H}'^H(f)\mathbf{d}\left(f,1\right)&=\left[\begin{array}{cccc}1 & e^{-\jmath 2\pi f\tau_0} & \cdots & e^{-\jmath(M-N-1)2\pi f\tau_0}\end{array}\right]^T \\ &=\widetilde{\mathbf{d}}\left(f,1\right).\end{aligned} \tag{64}$$

As a result, the distortionless constraint for the filter $\mathbf{h}(f)$ or, equivalently, the filter $\mathbf{g}(f)$ is

$$\mathbf{h}^H(f)\mathbf{d}(f,1) = \mathbf{g}^H(f)\widetilde{\mathbf{d}}(f,1) = 1. \tag{65}$$

Using (60), we can express the WNG and the beampattern as, respectively,

$$\begin{aligned}\mathcal{W}[\mathbf{h}(f)] &= \frac{\left|\mathbf{h}^H(f)\mathbf{d}(f,1)\right|^2}{\mathbf{h}^H(f)\mathbf{h}(f)} \\ &= \frac{\left|\mathbf{g}^H(f)\widetilde{\mathbf{d}}(f,1)\right|^2}{\mathbf{g}^H(f)\mathbf{H}'^H(f)\mathbf{H}'(f)\mathbf{g}(f)} \\ &= \mathcal{W}[\mathbf{g}(f)]\end{aligned} \tag{66}$$

and

$$\begin{aligned}\mathcal{B}\left[\mathbf{h}(f),\cos\theta\right] &= \mathbf{d}^H\left(f,\cos\theta\right)\mathbf{h}(f)\\ &= \mathbf{d}^H\left(f,\cos\theta\right)\mathbf{H}'(f)\mathbf{g}(f)\\ &= \mathcal{B}\left[\mathbf{g}(f),\cos\theta\right].\end{aligned} \tag{67}$$

With the proposed approach, the best way to improve the robustness of the filter with respect to white noise amplification is to maximize the WNG as given in (66), i.e.,

$$\min_{\mathbf{g}(f)} \mathbf{g}^H(f)\mathbf{H}'^H(f)\mathbf{H}'(f)\mathbf{g}(f) \quad \text{subject to} \quad \mathbf{g}^H(f)\widetilde{\mathbf{d}}\left(f,1\right)=1. \tag{68}$$

We obtain the maximum WNG (MWNG) filter:

$$\mathbf{g}_{\mathrm{MWNG}}(f)=\frac{\left[\mathbf{H}'^H(f)\mathbf{H}'(f)\right]^{-1}\widetilde{\mathbf{d}}\left(f,1\right)}{\widetilde{\mathbf{d}}^H\left(f,1\right)\left[\mathbf{H}'^H(f)\mathbf{H}'(f)\right]^{-1}\widetilde{\mathbf{d}}\left(f,1\right)}. \tag{69}$$

As a result, the global MWNG filter is

$$\mathbf{h}_{\mathrm{MWNG}}(f) = \mathbf{H}'(f)\mathbf{g}_{\mathrm{MWNG}}(f). \tag{70}$$

This filter is equivalent to the robust filter, $\mathbf{h}_{\mathrm{R}}(f)$.

While $\mathbf{h}_{\mathrm{MWNG}}(f)$ greatly improves the WNG, the designed beampattern diverges from the desired one as the frequency increases.

Figures 20 displays the patterns [with $\mathbf{h}_{\mathrm{MWNG}}(f)$ defined in (70)] of the first-order supercardioid for $f = 1$ kHz, $\delta = 0.5$ cm, and several values of M.

Figure 21 shows plots of the DF and WNG, $\mathcal{D}\left[\mathbf{h}_{\mathrm{MWNG}}(f)\right]$ and $\mathcal{W}\left[\mathbf{h}_{\mathrm{MWNG}}(f)\right]$ for the first-order supercardioid.

We observe that the WNG is considerably improved as M increases, while the beampatterns and the DFs do not change much.

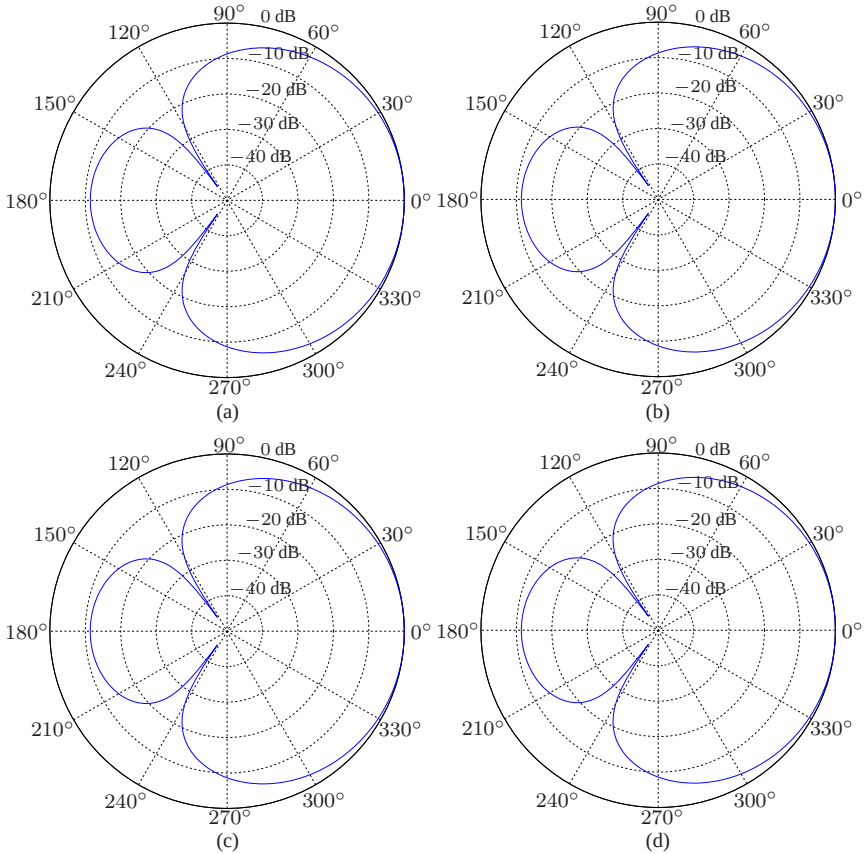

Figure 20: Beampatterns of the MWNG first-order supercardioid for $f = 1$ kHz, $\delta = 0.5$ cm, and several values of M: (a) $M = 3$, (b) $M = 4$, (c) $M = 6$, and (d) $M = 8$.

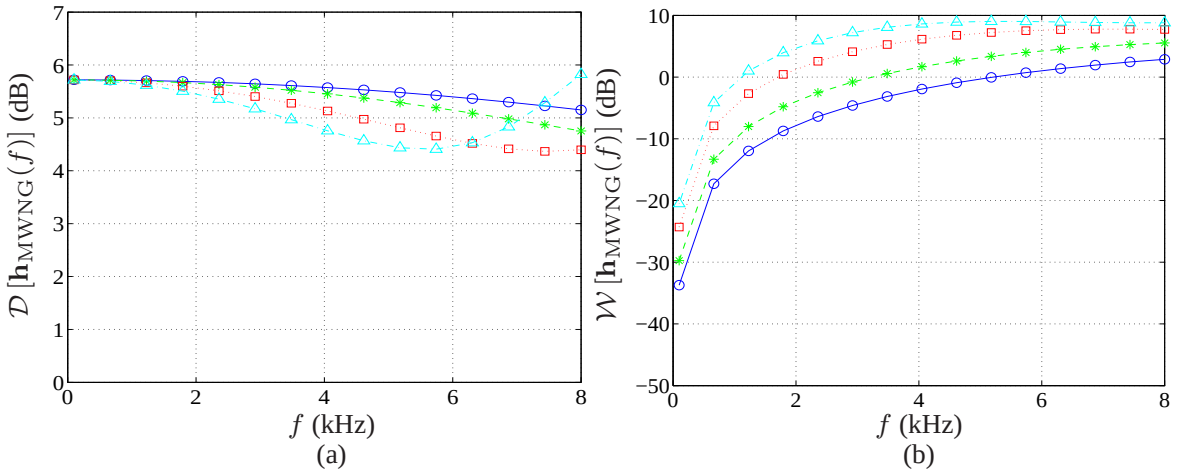

Figure 21: (a) DF and (b) WNG of the MWNG first-order supercardioid as a function of frequency, for $\delta = 0.5$ cm and several values of M: $M = 3$ (solid line with circles), $M = 4$ (dashed line with asterisks), $M = 6$ (dotted line with squares), and $M = 8$ (dash-dot line with triangles).

Constrained LS Filter

Let us define the error signal between the array beampattern and the desired directivity pattern:

$$\begin{aligned}\mathcal{E}\left[\mathbf{h}(f),\cos\theta\right] &= \mathcal{B}\left[\mathbf{h}(f),\cos\theta\right]-\mathcal{B}\left(\mathbf{b}_N,\cos\theta\right) \\ &= \mathbf{d}^H\left(f,\cos\theta\right)\mathbf{H}'(f)\mathbf{g}(f)-\mathbf{p}_{\mathrm{C}}^T\left(\cos\theta\right)\mathbf{b}_N \\ &= \mathcal{E}\left[\mathbf{g}(f),\cos\theta\right].\end{aligned} \tag{71}$$

The LSE criterion can be expressed as

$$\begin{aligned}\mathrm{LSE}\left[\mathbf{g}(f)\right] &= \frac{1}{\pi}\int_0^{\pi}\left|\mathcal{E}\left[\mathbf{g}(f),\cos\theta\right]\right|^2 d\theta \\ &= \mathbf{g}^H(f)\mathbf{H}'^H(f)\mathbf{\Gamma}_{\mathrm{C}}(f)\mathbf{H}'(f)\mathbf{g}(f)-\mathbf{g}^H(f)\mathbf{H}'^H(f)\mathbf{\Gamma}_{\mathbf{dp}_{\mathrm{C}}}(f)\mathbf{b}_N \\ &\quad -\mathbf{b}_N^T\mathbf{\Gamma}_{\mathbf{dp}_{\mathrm{C}}}^H(f)\mathbf{H}'(f)\mathbf{g}(f)+\mathbf{b}_N^T\mathbf{M}_{\mathrm{C}}\mathbf{b}_N.\end{aligned} \tag{72}$$

In order to get frequency-invariant beampatterns, we can minimize the LSE criterion subject to the distortionless constraint, i.e.,

$$\min_{\mathbf{g}(f)} \mathrm{LSE}\left[\mathbf{g}(f)\right] \quad \text{subject to} \quad \mathbf{g}^H(f)\widetilde{\mathbf{d}}\left(f,1\right) = 1, \tag{73}$$

from which we deduce the constrained LS (CLS) filter:

$$\mathbf{g}_{\mathrm{CLS}}(f) = \mathbf{g}_{\mathrm{LS}}(f) + \frac{1 - \widetilde{\mathbf{d}}^H\left(f,1\right)\mathbf{g}_{\mathrm{LS}}(f)}{\widetilde{\mathbf{d}}^H\left(f,1\right)\mathbf{R}^{-1}(f)\widetilde{\mathbf{d}}\left(f,1\right)}\mathbf{R}^{-1}(f)\widetilde{\mathbf{d}}\left(f,1\right), \tag{74}$$

where

$$\mathbf{g}_{\mathrm{LS}}(f) = \mathbf{R}^{-1}(f)\mathbf{H}'^H(f)\mathbf{\Gamma}_{\mathbf{dp}_{\mathrm{C}}}(f)\mathbf{b}_N \tag{75}$$

is the LS filter obtained by minimizing $\mathrm{LSE}\left[\mathbf{g}(f)\right]$ and

$$\mathbf{R}(f) = \mathbf{H}'^H(f)\mathbf{\Gamma}_{\mathrm{C}}(f)\mathbf{H}'(f). \tag{76}$$

As a result, the global CLS filter is

$$\mathbf{h}_{\mathrm{CLS},2}(f) = \mathbf{H}'(f)\mathbf{g}_{\mathrm{CLS}}(f). \tag{77}$$

This filter is mostly equivalent to $\mathbf{h}_{\mathrm{CLS}}(f)$.

While $\mathbf{h}_{\mathrm{CLS},2}(f)$ leads to very nice frequency-invariant responses, it severely suffers from white noise amplification.

Figures 22 displays the patterns [with $\mathbf{h}_{\mathrm{CLS},2}(f)$ defined in (77)] of the first-order supercardioid for $f = 1$ kHz, $\delta = 0.5$ cm, and several values of M.

Figure 23 shows corresponding plots of the DF and WNG.

We observe that the beampatterns and the DFs are approximately frequency invariant, but the WNG is very low, and becomes even worse as M increases.

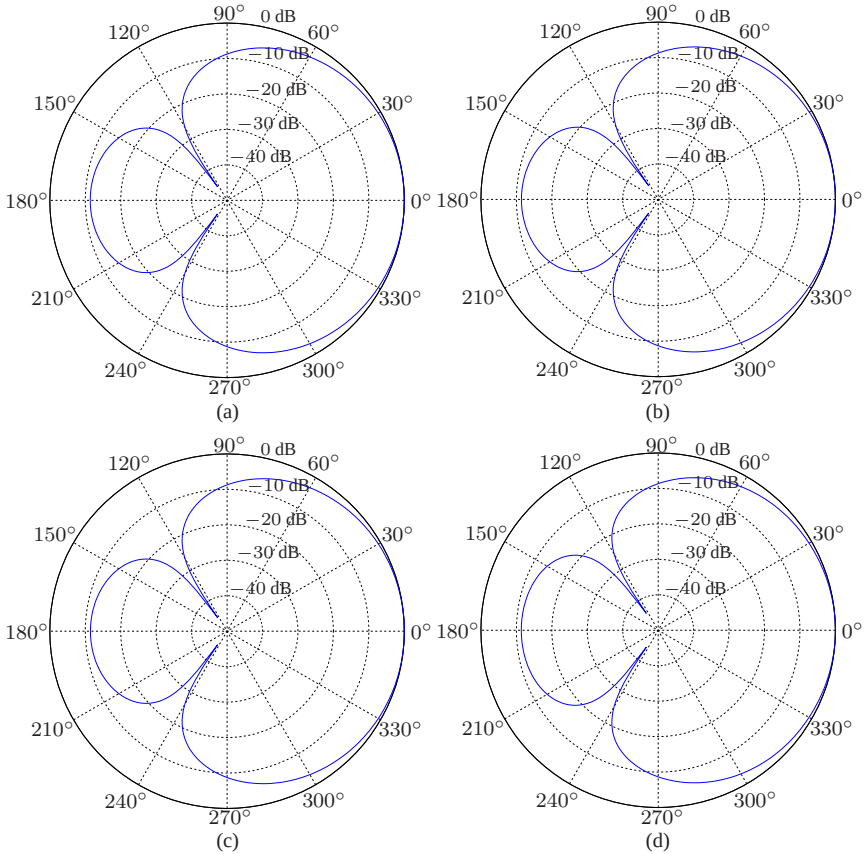

Figure 22: Beampatterns of the CLS first-order supercardioid for $f = 1$ kHz, $\delta = 0.5$ cm, and several values of M: (a) $M = 3$, (b) $M = 4$, (c) $M = 6$, and (d) $M = 8$.

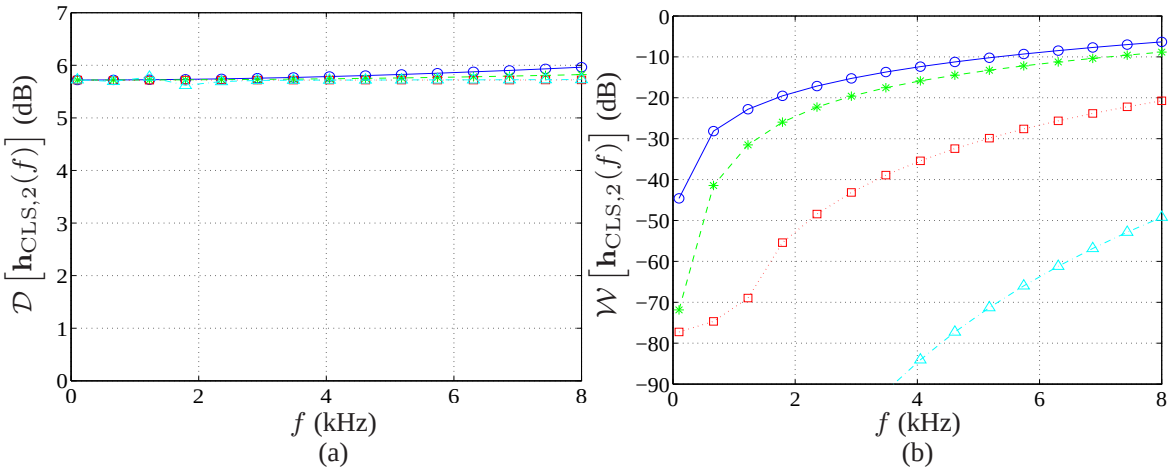

Figure 23: (a) DF and (b) WNG of the CLS first-order supercardioid as a function of frequency, for $\delta = 0.5$ cm and several values of M: $M = 3$ (solid line with circles), $M = 4$ (dashed line with asterisks), $M = 6$ (dotted line with squares), and $M = 8$ (dash-dot line with triangles).

Tradeoff Filter

In order to compromise between the WNG and frequency-invariant beampatterns, we should jointly optimize the two previous approaches.

Let us define the criterion:

$$J_{\aleph}\left[\mathbf{g}(f)\right] = \aleph \mathrm{LSE}\left[\mathbf{g}(f)\right] + (1-\aleph)\mathbf{g}^H(f)\mathbf{H}'^H(f)\mathbf{H}'(f)\mathbf{g}(f), \qquad (78)$$

where $\aleph \in [0,1]$ controls the tradeoff between the WNG and the error beampattern.

Taking into account the distortionless constraint, the optimization problem is

$$\min_{\mathbf{g}(f)} J_{\aleph}\left[\mathbf{g}(f)\right] \quad \text{subject to} \quad \mathbf{g}^H(f)\widetilde{\mathbf{d}}\left(f,1\right) = 1. \qquad (79)$$

We find that the tradeoff filter is

$$\mathbf{g}_{\mathrm{T},\aleph}(f) = \mathbf{g}_{\mathrm{U},\aleph}(f) + \frac{1 - \widetilde{\mathbf{d}}^H(f,1)\,\mathbf{g}_{\mathrm{U},\aleph}(f)}{\widetilde{\mathbf{d}}^H(f,1)\,\mathbf{R}_{\aleph}^{-1}(f)\widetilde{\mathbf{d}}(f,1)}\mathbf{R}_{\aleph}^{-1}(f)\widetilde{\mathbf{d}}(f,1), \quad (80)$$

where

$$\mathbf{g}_{\mathrm{U},\aleph}(f) = \aleph\mathbf{R}_{\aleph}^{-1}(f)\mathbf{H}'^H(f)\mathbf{\Gamma}_{\mathbf{dp}_\mathrm{C}}(f)\mathbf{b}_N \quad (81)$$

is the unconstrained filter obtained by minimizing $J_\aleph[\mathbf{g}(f)]$ and

$$\mathbf{R}_\aleph(f) = \aleph\mathbf{R}(f) + (1-\aleph)\mathbf{H}'^H(f)\mathbf{H}'(f). \quad (82)$$

Consequently, the global tradeoff filter from the proposed joint optimization is

$$\mathbf{h}_{\mathrm{T},\aleph}(f) = \mathbf{H}'(f)\mathbf{g}_{\mathrm{T},\aleph}(f). \quad (83)$$

Obviously, in the two extreme cases, we have $\mathbf{h}_{\mathrm{T},0}(f) = \mathbf{h}_{\mathrm{MWNG}}(f)$ and $\mathbf{h}_{\mathrm{T},1}(f) = \mathbf{h}_{\mathrm{CLS},2}(f)$.

Figures 24 displays the patterns [with $\mathbf{h}_{\mathrm{T},\aleph}(f)$ defined in (83)] of the first-order supercardioid for $f = 1$ kHz, $\delta = 0.5$ cm, $M = 6$, and several values of $\aleph$.

Figure 25 shows corresponding plots of the DF and WNG.

We observe that $\aleph$ compromises between the WNG and frequency-invariant beampatterns.

The DF at high frequencies is improved as $\aleph$ increases, while the WNG is significantly higher than that with $\mathbf{h}_{\mathrm{CLS},2}(f)$.

Compared to the CLS filter, the jointly optimized filter is considerably more robust against white noise amplification, but leads to slightly less frequency-invariant responses.

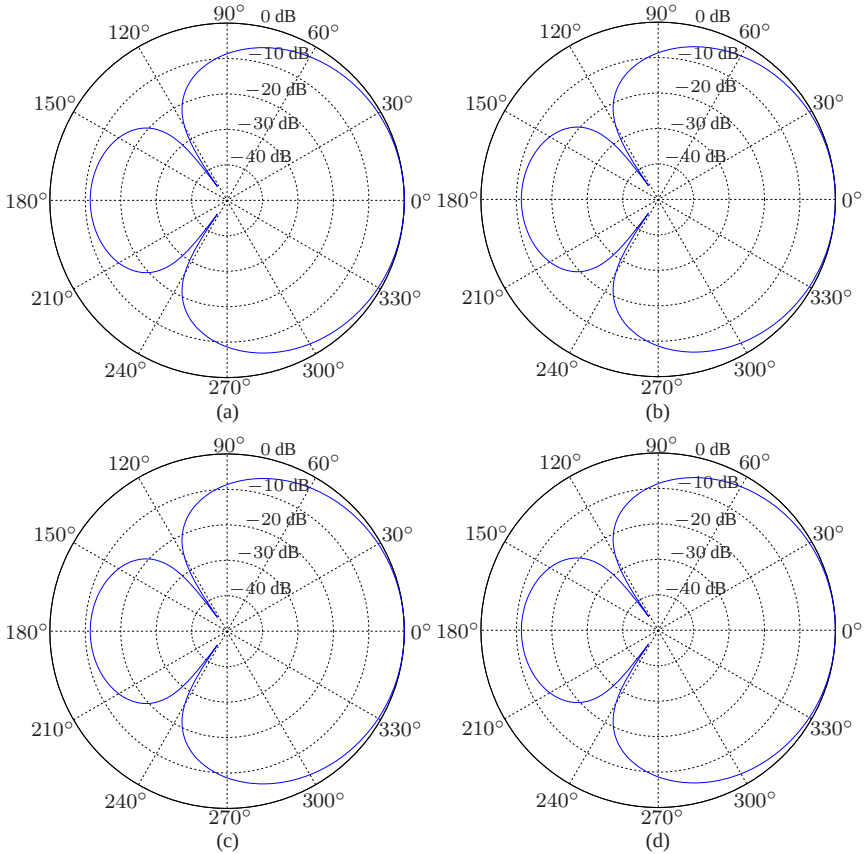

Figure 24: Beampatterns of the jointly optimized first-order supercardioid for $f = 1$ kHz, $\delta = 0.5$ cm, $M = 6$, and several values of $\aleph$: (a) $\aleph = 0$, (b) $\aleph = 0.5$, (c) $\aleph = 0.9$, and (d) $\aleph = 0.99$.

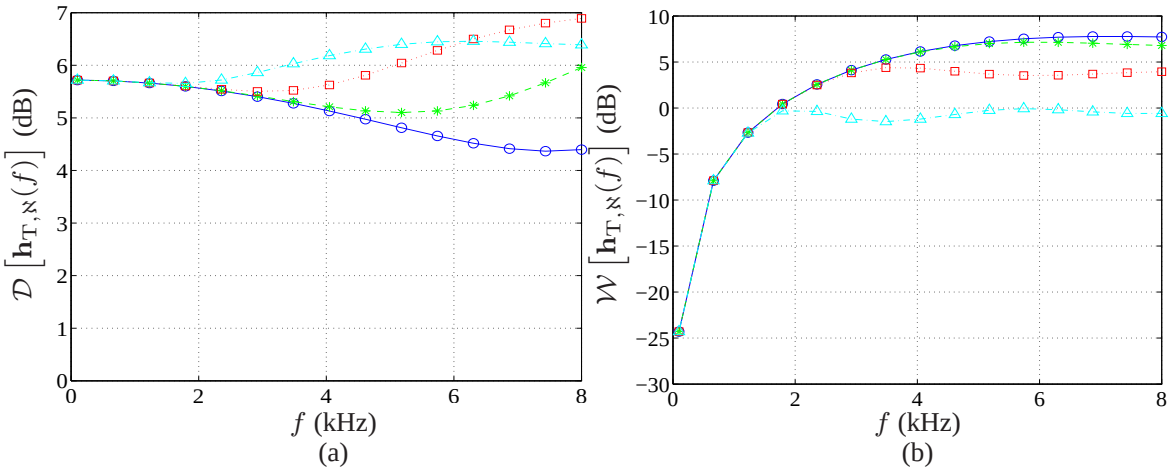

Figure 25: (a) DF and (b) WNG of the jointly optimized first-order supercardioid as a function of frequency, for $\delta = 0.5$ cm, $M = 6$, and several values of $\aleph$: $\aleph = 0$ (solid line with circles), $\aleph = 0.5$ (dashed line with asterisks), $\aleph = 0.9$ (dotted line with squares), and $\aleph = 0.99$ (dash-dot line with triangles).

Table 1: Filters for beampattern design.

Nonrobust:	$\mathbf{h}_{\mathrm{NR}}(f) = \overline{\mathbf{B}}_{M-1}^{-1}(f)\mathbf{b}_{M-1}$
Robust:	$\mathbf{h}_{\mathrm{R}}(f) = \overline{\mathbf{B}}_N^H(f)\left[\overline{\mathbf{B}}_N(f)\overline{\mathbf{B}}_N^H(f)\right]^{-1}\mathbf{b}_N$
Freq.-inv.:	$\mathbf{h}_{\mathrm{FI}}(f) = \mathbf{\Gamma}_{\mathrm{C}}^{-1}(f)\overline{\mathbf{B}}_N^H(f)\left[\overline{\mathbf{B}}_N(f)\mathbf{\Gamma}_{\mathrm{C}}^{-1}(f)\overline{\mathbf{B}}_N^H(f)\right]^{-1}\mathbf{b}_N$
	$\mathbf{h}_{\mathrm{FI},\epsilon}(f) = \mathbf{\Gamma}_{\mathrm{C},\epsilon}^{-1}(f)\overline{\mathbf{B}}_N^H(f)\left[\overline{\mathbf{B}}_N(f)\mathbf{\Gamma}_{\mathrm{C},\epsilon}^{-1}(f)\overline{\mathbf{B}}_N^H(f)\right]^{-1}\mathbf{b}_N$
LS:	$\mathbf{h}_{\mathrm{LS}}(f) = \mathbf{\Gamma}_{\mathrm{C}}^{-1}(f)\mathbf{\Gamma}_{\mathbf{dp}_{\mathrm{C}}}(f)\mathbf{b}_N$
	$\mathbf{h}_{\mathrm{LS},\epsilon}(f) = \mathbf{\Gamma}_{\mathrm{C},\epsilon}^{-1}(f)\mathbf{\Gamma}_{\mathbf{dp}_{\mathrm{C}}}(f)\mathbf{b}_N$
	$\mathbf{h}_{\mathrm{CLS}}(f) = \mathbf{h}_{\mathrm{LS}}(f) - \dfrac{1-\mathbf{d}^H(f,1)\,\mathbf{h}_{\mathrm{LS}}(f)}{\mathbf{d}^H(f,1)\,\mathbf{\Gamma}_{\mathrm{C}}^{-1}(f)\mathbf{d}(f,1)}\mathbf{\Gamma}_{\mathrm{C}}^{-1}(f)\mathbf{d}(f,1)$
	$\mathbf{h}_{\mathrm{CLS},\epsilon}(f) = \mathbf{h}_{\mathrm{LS},\epsilon}(f) - \dfrac{1-\mathbf{d}^H(f,1)\,\mathbf{h}_{\mathrm{LS},\epsilon}(f)}{\mathbf{d}^H(f,1)\,\mathbf{\Gamma}_{\mathrm{C},\epsilon}^{-1}(f)\mathbf{d}(f,1)}\mathbf{\Gamma}_{\mathrm{C},\epsilon}^{-1}(f)\mathbf{d}(f,1)$
	$\mathbf{h}_{\mathrm{CLS},2}(f) = \mathbf{H}'(f)\mathbf{g}_{\mathrm{CLS}}(f)$
Max. WNG:	$\mathbf{h}_{\mathrm{MWNG}}(f) = \dfrac{\mathbf{H}'(f)\left[\mathbf{H}'^H(f)\mathbf{H}'(f)\right]^{-1}\widetilde{\mathbf{d}}(f,1)}{\widetilde{\mathbf{d}}^H(f,1)\left[\mathbf{H}'^H(f)\mathbf{H}'(f)\right]^{-1}\widetilde{\mathbf{d}}(f,1)}$
Joint opt.:	$\mathbf{h}_{\mathrm{T},\aleph}(f) = \mathbf{H}'(f)\mathbf{g}_{\mathrm{T},\aleph}(f)$

[1] H. F. Davis, *Fourier Series and Orthogonal Functions*. New York: Dover, 1989.

[2] L. Zhao, J. Benesty, and J. Chen, "Optimal design of directivity patterns for endfire linear microphone arrays," in *Proc. IEEE ICASSP*, 2015, pp. 295–299.

[3] L. Zhao, J. Benesty, and J. Chen, "Design of robust differential microphone arrays with the Jacobi-Anger expansion," *Applied Acoustics*, vol. 110, pp. 194–206, Sept. 2016.

[4] M. Abramowitz and I. A. Stegun, Eds., *Handbook of Mathematical Functions with Formulas, Graphs, and Mathematical Tables*. New York: Dover, 1970.

[5] C. Pan, J. Benesty, and J. Chen, "Design of robust differential microphone arrays with orthogonal polynomials," *J. Acoust. Soc. Am.*, vol. 138, pp. 1079–1089, Aug. 2015.

[6] D. Colton and R. Krees, *Inverse Acoustics and Electromagnetic Scattering Theory*. Second Edition, Berlin, Germany: Springer-Verlag, 1998.

[7] A. Cuyt, V. B. Petersen, B. Verdonk, H. Waadeland, and W. B. Jones, *Handbook of Continued Fractions for Special Functions*. Berlin, Germany: Springer-Verlag, 2008.

[8] G. W. Elko, “Superdirectional microphone arrays,” in *Acoustic Signal Processing for Telecommunication*, S. L. Gay and J. Benesty, Eds. Boston, MA: Kluwer Academic Publishers, 2000, Chapter 10, pp. 181–237.

[9] J. Benesty and J. Chen, *Study and Design of Differential Microphone Arrays*. Berlin, Germany: Springer-Verlag, 2012.